Unveiling Superconductivity in Two-dimensional Nb$_2$C MXene with Highest Critical Temperature (T$_c$)

Zaheer-Ud-Din Babar
Fall-2017-MS Physics
Reg. # 00000203217

A thesis submitted in partial fulfillment of the requirements for the degree of **Master of Science**

In

Physics

Supervised by:

Dr. Syed Rizwan Hussain

Co-supervised by:

Dr. Mudassar Iqbal

Department of Physics
School of Natural Sciences (SNS)
National University of Sciences and Technology (NUST)
H-12, Islamabad, Pakistan
Year 2019

National University of Sciences & Technology

MS THESIS WORK

We hereby recommend that the dissertation prepared under our supervision by: Zaheer ud Din Babar, Regn No. 00000203217 Titled: **Unveiling Superconductivity in Two-dimensional Nb$_2$C MXene with Highest Critical Temperature (Tc)** accepted in partial fulfillment of the requirements for the award of **MS** degree.

Examination Committee Members

1. Name: DR. FAHEEM AMIN _____ Signature: _____ .

2. Name: DR. MANZAR SOHAIL _____ Signature: _____ .

External Examiner: DR. MUHAMMAD MUMTAZ   Signature: _____ .

Supervisor's Name DR. SYED RIZWAN HUSSAIN   Signature: _____ .

CO-Supervisor's Name DR. MUDASSIR IQBAL   Signature: _____ .

_____
Head of Department

_____
27/08/19
Date

COUNTERSINGED

_____
Dean/Principal

Date: 27/8/2019

THESIS ACCEPTANCE CERTIFICATE

Certified that final copy of MS thesis written by **Mr. Zaheer ud Din Babar** (Registration No. **00000203217**), of **School of Natural Sciences** has been vetted by undersigned, found complete in all respects as per NUST statutes/regulations, is free of plagiarism, errors, and mistakes and is accepted as partial fulfillment for award of MS/M.Phil degree. It is further certified that necessary amendments as pointed out by GEC members and external examiner of the scholar have also been incorporated in the said thesis.

Signature: _____

Name of Supervisor: Dr. Syed Rizwan Hussain

Date: _____27/08/19_____

Signature (HoD): _____

Date: _____27/08/19_____

Signature (Dean/Principal): _____

Date: _____27/8/2019_____

Dedicated

To

My Late Sister

"May Allah (SWT) Grants Her Highest Rank in Jannah"

Acknowledgements

Abstract

Magnetism in two-dimensional (2D) materials is a forefront topic in today's research due to their promising technological applications in data storage, spintronic devices and many more. More importantly, the superconductivity in two dimensional materials has garnered a tremendous attention of the world research community and a lot of efforts are being made to fabricate 2-D superconductors. In 2011, the synthesis of new class of two-dimensional materials known as MXenes ($M_{n+1}X_n$) at Drexel University, Philadelphia, has auctioned the possibility of magnetism in new 2D materials and their possible uses in spintronics. The systematic synthesis process at such 2D MXene is described to produce nanoscale Nb_2CTx-MXene under optimized temperature and time using wet chemical etching route. The X-ray diffraction indicates significant increase in c-lattice parameter from 13.83Å to 22.72Å indicating successful etching and intercalation of MXene sheets. A typical 2D layered morphology can be seen through SEM images with well-defined lamellar structure. The Raman spectra indicate that MXene structure is more ordered with less defect densities. Magnetic measurements of as-synthesized MXene powder unveil the existance of Type-II superconductivity. Magnetization vs. Temperature (MT) indicates a phase transition from normal to superconducting state at T_c^{onset}(K)=12.5K with splitting between ZFC-FC curve at low temperature with negative magnetization (superconducting diamagnetism) at low temperature due the formation of so called vortex state in Type-II superconductors. This superconducting diamagnetism can be seen more prominently from Magnetization vs. Field (M-H) curves with broader Loops at low temperature. The experimental results are well fitted with Ginzburg-Landau (GL) theory of type-II superconductors. Thus as-prepared Nb_2C-MXene is a type-II superconductor with T_c^{onset} (K) =12.5K. Moreover, Current density (Jc) also satisfies the superconducting behavior in Nb_2C-MXene Powder. Thus, this work is a significant development towards the existance of superconductivity in 2D materials, thus opening a door towards high temperature 2D superconducting Spintronics.

Thesis Layout

The layout of the thesis is as follows;

Chapter 01

In this chapter, a brief introduction of nano structured materials is presented with brief introduction of superconductivity as well.

Chapter 02

This chapter contains a detailed literature survey about MXene phases and superconductivity in other MAX/MXene phases, includes synthesis of Nb_2C MXene with its different applications.

Chapter 03

Third chapter governs the systematic synthesis etching process and details of characterizations carried out in this work.

Chapter 04

This chapter contains all the results and discussion on the existance of superconductivity in Nb_2C MXene.

Chapter 05

A detailed summery of the thesis is presented with conclusive remarks on this project.

List of Figures

List of Tables

Contents

Chapter 1 Introduction

1.1 What is nano science and nano technology?

The Greek originated word *nano* means "dwarf" and it is one billionth of a meter, 1nm = 10^{-9} m. The simplest description of nano technology is the "Technology at nano scale" and it is the study of extremely small objects at smaller scale. The main feature of the nanotechnology includes design/device fabrication, synthesis, manipulation and application of different materials with at least one dimension in the range of 0.1-100-nm. So, objects being included in nanotechnology regime are presumed to own one or more dimension (length/width/height) at nanoscale. [1, 2] The material at Nano scale has mechanical, optical, magnetic and electrical properties which are different from the material at their bulk scale. The difference in their properties at nanoscale mainly includes the large surface area, large surface to volume ratio and enhanced quantum confinement effects. [3]

1.2 History of Nano Sciences and Technology

For the first time, *Richard Zsigmondy* proposed the idea of nano technology (Nobel Laurette in Chemistry, 1925), by giving the term *"nanometer"* by characterizing the particle size of gold colloidal by using microscope. [4]

The introduction to nano technology is often credited to the *Richard P. Feynman* (Nobel Laurette in Physics, 1965); almost 50 years ago he delivered a well-known lecture, entitled ***"There Is a Plenty of Room at the Bottom"*** at California institute of Technology during annual meeting of American Physical Society. Nowadays this lecture of Feynman is recognized as the origin of Nanotechnology. [5]

Marvin Minsky gave a similar idea; "clearly it is viable to have complex machines with dimensions comparable to a flea, possibly one can have them to the size of bacteria cells." [6]

In 1974, the word "nanotechnology" was first introduced to world at international conference of industrial production at Tokyo Japan by N. Taniguchi (a professor at the Tokyo University of Science) talking about processing of nanomaterials with high accuracy to nano scales. [7]

"Engines of creation: the arrival of nanotechnology era" by Eric Drexler published in September 1986, giving a profound insight to Nano technological strategy and its enormous implications. [8]

After this book, Drexler established a foresight institute with the aim to the fortify the favorable implication of nano technology as what he proposed in his book and this institute further propagated the research in this era.[9]

First Nano technological program of national scientific fund operated by USA initiates its work in 1991. Also In 2001, USA approved the National Nano technological Initiative (NNI) with a motivation of nanotechnology development and becoming at useful source of USA economy till first half of 21st century. [4]

Onwards a lot of research and development has been done this era from the synthesis of lot of promising materials e.g. graphene (a Miracle material) to MXene (2D transition metal carbide) and their applications to various fields. [10, 11, 12, 13]

1.3 Requirements of Nanotechnology

Nanomaterials have tremendous range of demand in many fields of engineering and basic sciences. It is important to note that their applications are mainly based upon many factors such as particle size & dimensions, surface to volume ratio, surface area and many other physical and chemical properties that effectively manipulate and provide room for the versatile requirements.

Sectors where nano technology have significant impacts: [14]

- ❖ Electronics and optoelectronics, photonic
- ❖ Bio-nanotechnology and bio-sensors
- ❖ Energy sector, including fuel cells, batteries and photovoltaics
- ❖ Environment sector including water remediation
- ❖ Composite materials
- ❖ Construction sector, including reinforcement of materials
- ❖ Medical and pharmaceutical sector
- ❖ Aeronautics and Automotive sector

1.4 Nano materials

As defined earlier, a nano material is a material with at least one dimension in the range of 0.1-100nm. So, objects being included in nanotechnology regime are presumed to own one or more dimension (length/width/height) at nanoscale. Their

physical and chemical properties are much different as compared to their bulk scale which makes the favorable for many applications such as magnetic storage media, spintronics and many more. [15]

1.4.1 Classification of nano Structured Materials (NSM's)

The idea of Nano structured materials NMS's was firstly given by Gleiter (1995) and was further illustrated by Skorokhod (2000), at that time scheme was not completely accepted because of 0D, 1D, 2D and 3D structure e.g. fullerenes, nano tubes and nano flowers were not included. So, Pokropivny and Skorokhod modified the classifications of nano materials. [16, 17]

A Nano material comes in different shapes, designs and dimensions. Depending upon these factors, nano materials are classified into following types.

- ❖ Zero dimensional (0D e.g. nanoparticles)
- ❖ One- dimensional (1D e.g. nanofibers, nano wires)
- ❖ Two-dimensional (2D e.g. nano sheets, thin films)
- ❖ Three-dimensional (3D e.g. Nano flowers, nano structure)
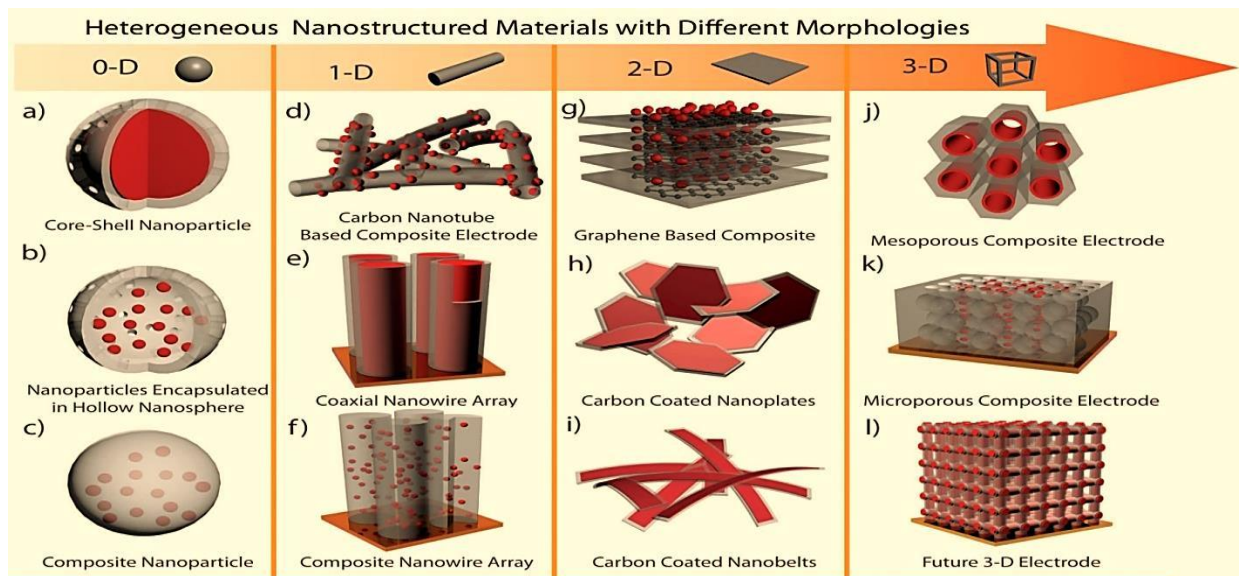
Figure 1.1: A brief pictorial presentation [18]

1.4.1.1 Zero-Dimensional (0-D)

In Zero dimensional nano particles, electrons are confined in all direction. They are not allowed to move anywhere inside the system. Such particles with size ≤ 100 nm have nano dimensions in all their directions. Examples are quantum dots, nano rings, nano shells and nano particles encapsulated in Hollow nano spheres etc.

1.4.1.2 One-Dimensional (1-D)

In one dimensional nano particles, electrons are just confined in any of the two directions. These particles consist of one direction in macroscale and one dimension in nanoscale and electrons are only allowed to move in only single directions. Examples are carbon nano tubes, nano layers, nano coatings and composite nanowire arrays etc.

1.4.1.3 Two-Dimensional (2-D)

Electrons are restricted in any of the two directions in 2D nano particles. These particles consist of one direction in macroscale and electrons are allowed to move in one direction. Examples are thin films, graphene based composites, carbon coated Nano plates, layered transition metal carbides knowns as MXenes and carbon coated nano belts etc.

1.4.1.4 Three-Dimensional (3-D)

Three dimensional nano particles are also known as bulk materials. These particles consist of all their direction in macroscale and electrons are allowed to move in all direction. These materials have not any directions at nano scale but have promising applications because of nano structures present in them. 3D nano materials consist of mesoporous composite electrode, clusters of nano wires or tubes and graphite etc.

1.5 Properties of Nano Structure Materials

It is worth noting when the object dimensions are smaller than the usual length of the charge carrier like phonons and electrons, the particles are certainly confined and laws of Quantum mechanics comes into play. Moreover, at such nano levels, their surface to volume ratio becomes high and their properties are affected by their surface properties rather than their bulk properties. The fallout of such surface effects and nano size significantly observed in electrical, electronic, optical, magnetic, chemical, semiconducting and thermal properties of nanomaterials. For example, two conductors that are placed on each side of insulator at nano dimensions, their electrons wave functions overlap and follow tunnel conduction. This became the basis of Scanning tunneling microscope and feasible of construct efficient magneto restrictive random access memory (MRAM). Now, redesigning the conducting materials by superconductors led the components of the SQUID (superconducting quantum interference device). [19]

1.6 Magnetic properties

Magnetization is defined as the response any material placed in a magnetic field. It is the extent to which a material in magnetized in the presence of that field and is the measure of net diploe moment per unit volume. It is notable that magnetic properties of nano particles are greatly dependent upon their dimensions and contain variety of unusual behavior. Magnetic properties of nano particles are considerably different from their bulk materials and therefore can be used to create novel devices and materials with new properties. They have important applications magnetic resonance imaging (MRI), in magnetic storage media, in biotechnology and targeted drug delivery. [20]

According to modern theories, the magnetic behavior in solids is due to the spin and orbital motion of electron and also attributed to the spin of nuclei. The motion of electron around the nucleus is analogous to the current that produces magnetic field. The main participant in the magnetism in the solids is the spins of number of unpaired electrons which produces the permanent magnetic moment inside them. These magnetic moments that are present in incomplete shells of an atom and unpaired electrons in the conduction band aligns themselves in random orientations thus giving a non-zero magnetic moment. [21]

1.6.1 Classification of magnetic materials

Depending upon the magnetic behavior, magnetic materials are divided into five classes

1) Diamagnetic materials
2) Paramagnetic materials
3) Ferro magnetic materials
4) Anti-ferromagnetic materials
5) Ferri magnetic materials

1.6.1.1 Diamagnetic materials

Diamagnetism is observed in solids that doesn't contain any permanent magnetic moments. It is a very weak effect and arises due to the presence of non-zero magnetic moments. These materials oppose the external field in which they are placed. In such materials, the spinning electrons change their orientation and producing a magnetization (**M**) by aligning themselves in the direction opposite to the applied field (**H**). Hence, the value their magnetic susceptibility (**χ**) (the degree of magnetization of a material in response to applied field) is negative. This effect exists almost in every

material but often dominated by the presence of stronger effects such as Para magnetism and diamagnetism. Examples are copper, silver and gold etc. [21, 22]
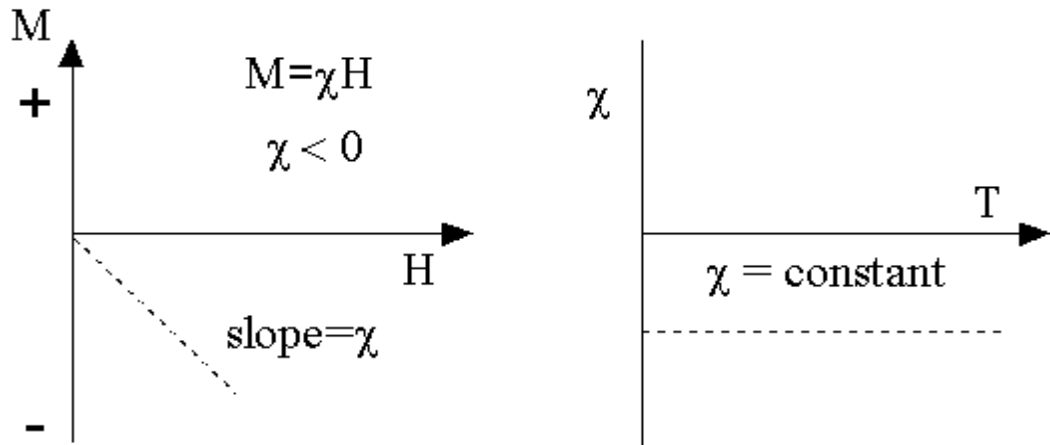
Figure 1.2: Diamagnetic susceptibility V/S applied field "H" and Temperature "T" [23]

1.6.1.2 Paramagnetic materials

Unlike diamagnetism, the magnetic moments of a paramagnetic material are aligned in the direction of external field. Paramagnetism is also a weak effect and the materials containing paramagnetic effect are attracted by the field in which they are placed. In the absence of the field, the magnetic moments of these materials are randomly oriented and do not have any net magnetic moments. Thus, the value of their magnetization is zero. Under the action of applied field (**H**), these moments align themselves in the field direction which results in its magnetization (**M**) on field direction. They have temperature dependent small and positive susceptibility (χ) value. Paramagnetism in observed in metals, gaseous nitride oxides and few compounds containing even no. of electrons e.g. Oxygen etc. [22]
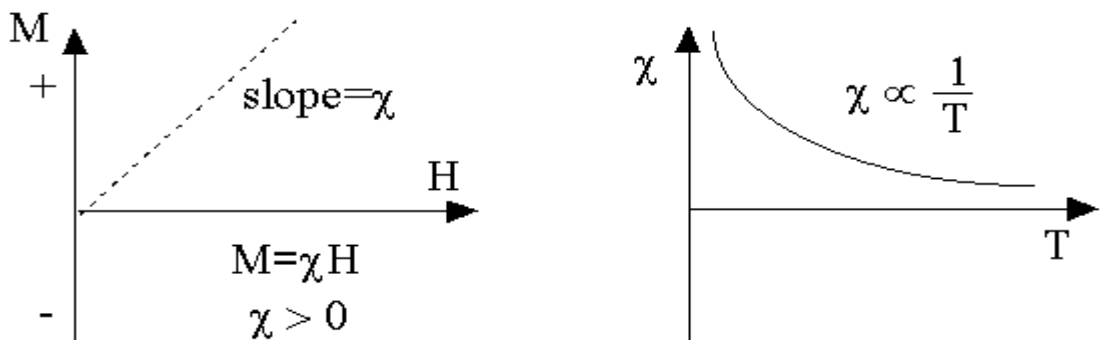
Figure 1.3: Paramagnetic susceptibility V/S applied field "H" and Temperature "T" [23]

1.6.1.3 Ferromagnetic materials

Ferromagnetism is strong magnetic effect and results when all magnetic moments are completely aligned in field direction. Like Paramagnetism, ferromagnetism is attributing to the presence of permanent magnetic moment. So, a ferromagnetic material discloses a net magnetic effect in the absence of external magnetic field. Such magnetization in the absence of the field is called spontaneous magnetization (M_S) which exists below a certain temperature called Curie temperature "Tc". The magnetization below this critical temperature occurs due to exchange interactions. After Curie temperature, such materials become paramagnet. There is a region of magnetic alignment known as "domains" formed by microscopic ordering of electron spin of ferromagnetic materials. Ferromagnetic materials have the ability to remain magnetized after subjection to magnetic field. This property to "remember the magnetic history" is called hysteresis. A related term is saturation magnetization that can be attained in field H_{sat}. This is the maximum extent to which a ferromagnet is magnetized; after this there is no increase in magnetization. After removal of field, a part of saturation magnetization is still present in such materials for some time called remanence of those materials. Common examples are Fe, Ni, Co, Gd and alloys such as MnBi, MnAs etc. [22-24]
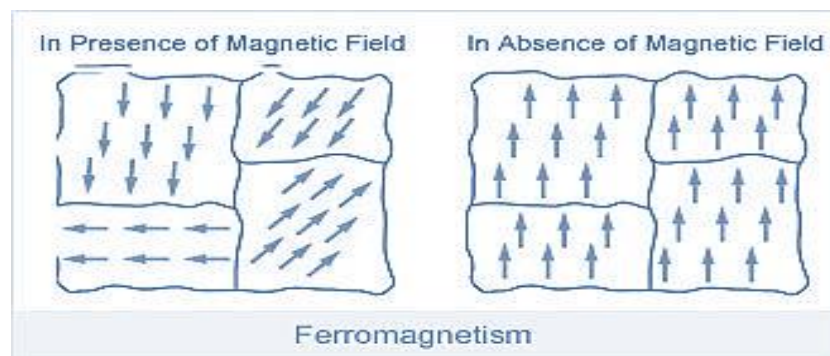
Figure 1.4: Domain orientations in Ferromagnetic materials [26]

1.6.1.4 Anti Ferromagnetic materials

In materials exhibiting anti-ferromagnetic consist of two adjacent/ interpenetrating sub lattices "A" and "B", in which one is spontaneously magnetized in one direction and other is magnetized in opposite direction. Such that, adjacent magnetic moments cancels each other effect in the absence of external applied field. This type of effect was first observed in MnO. When field is applied, the material is magnetized in field direction which increases with temperature and becomes supreme at certain

temperature called Neel's temperature analogous to Curie temperature in ferromagnet. After this temperature, there is significant decrease in magnetization which is evocative to the presence of paramagnetic state. [22]
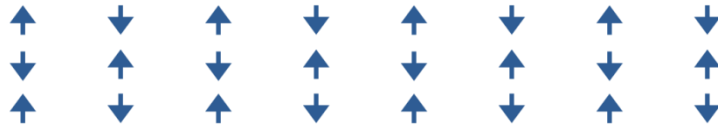
Figure 1.5: Anti-parallel orientations in anti-Ferromagnetic materials

1.6.1.5 Ferrimagnetic materials

The anti-ferromagnetism and ferrimagnetism are similar to each other expect the difference between that magnetization of the sub lattices have different values due to unequal magnetic moments. In Ferrimagnetic materials the moment of one sub lattice is half of the second sub lattice thus giving non-zero magnetization. This mostly occurs in ferrites, the most common example is ferrous ferrite, magnetite etc. [22]
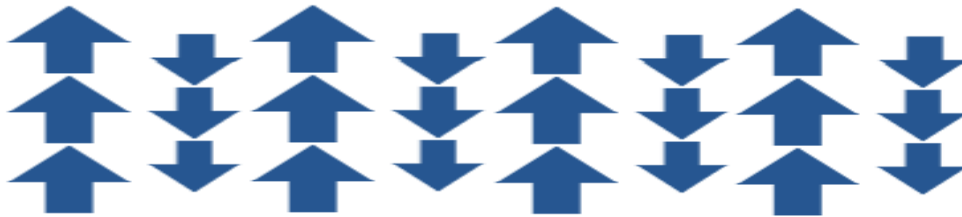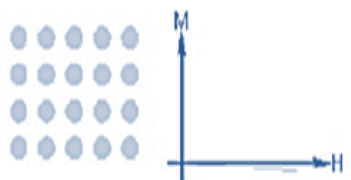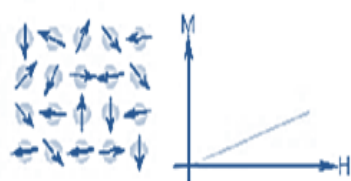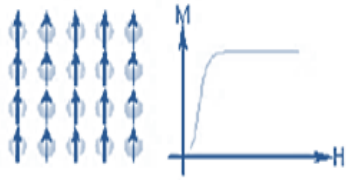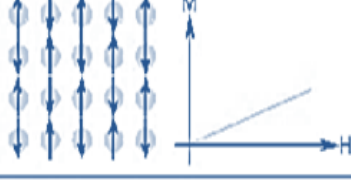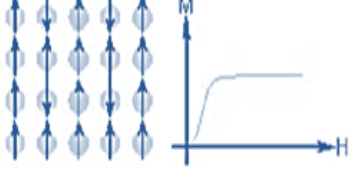
Figure 1.6: Anti-parallel orientations in Ferrimagnetic materials

1.7 Compact description of magnetic materials

There is compact classification of above all description of magnetic materials. [26]

Type of magnetism	Magnetic susceptibility, χ	Atomic / Magnetic Behavior	Temperature dependence	Examples and comments
Diamagnetic	Negative and small, Au: -2.74×10^{-6} Cu: -0.77×10^{-6}		Temperature independent	The shells of the atoms are closed as in the case of covalent solids such as Ge, Si, and metals such as Au, Cu, Ag, etc.
Paramagnetic	Positive and small, β-Sn: 0.19×10^{-6} Pt: 21.04×10^{-6} Mn: 66.10×10^{-6} 10^{-5}-10^{-4}		Temperature independent	Atoms have randomly oriented magnetic moments as in alkali and transition metals
	Positive and small		Follows Curie or Curie-Weiss law: $$\chi = \frac{C}{T-\theta}$$	Atoms constituting the material have a permanent magnetic moment as in ferromagnets (Fe), antiferromagnets (Cr), ferrimagnets (Fe_2O_3) at high temperatures
Ferromagnetic	Positive and large, function of applied field, microstructure dependent Fe: ~100,000		Ferromagnetic below Curie temperature and paramagnetic above it	Atoms have parallel aligned magnetic moments, possesses large permanent magnetization even without external magnetic field as in some transition metals and rare earths such as Fe, Co, Ni, Gd, Dy
Antiferromagnetic	Positive and small, Cr: 3.6×10^{-6}		Antiferromagnetic below the Néel temperature and paramagnetic above it	Atoms have mixed parallel and anti-parallel aligned magnetic moments Primarily oxides and salts of transition metals such as MnO, NiO, MnF_2.
Ferrimagnetic	Positive and large, function of applied field, microstructure dependent, Ba ferrite: ~3		Ferrimagnetic below the Curie temperature and paramagnetic above it	Atoms have anti-parallel aligned magnetic moments, possesses large magnetization even without external magnetic field

1.8 Brief Overview of application of nano materials
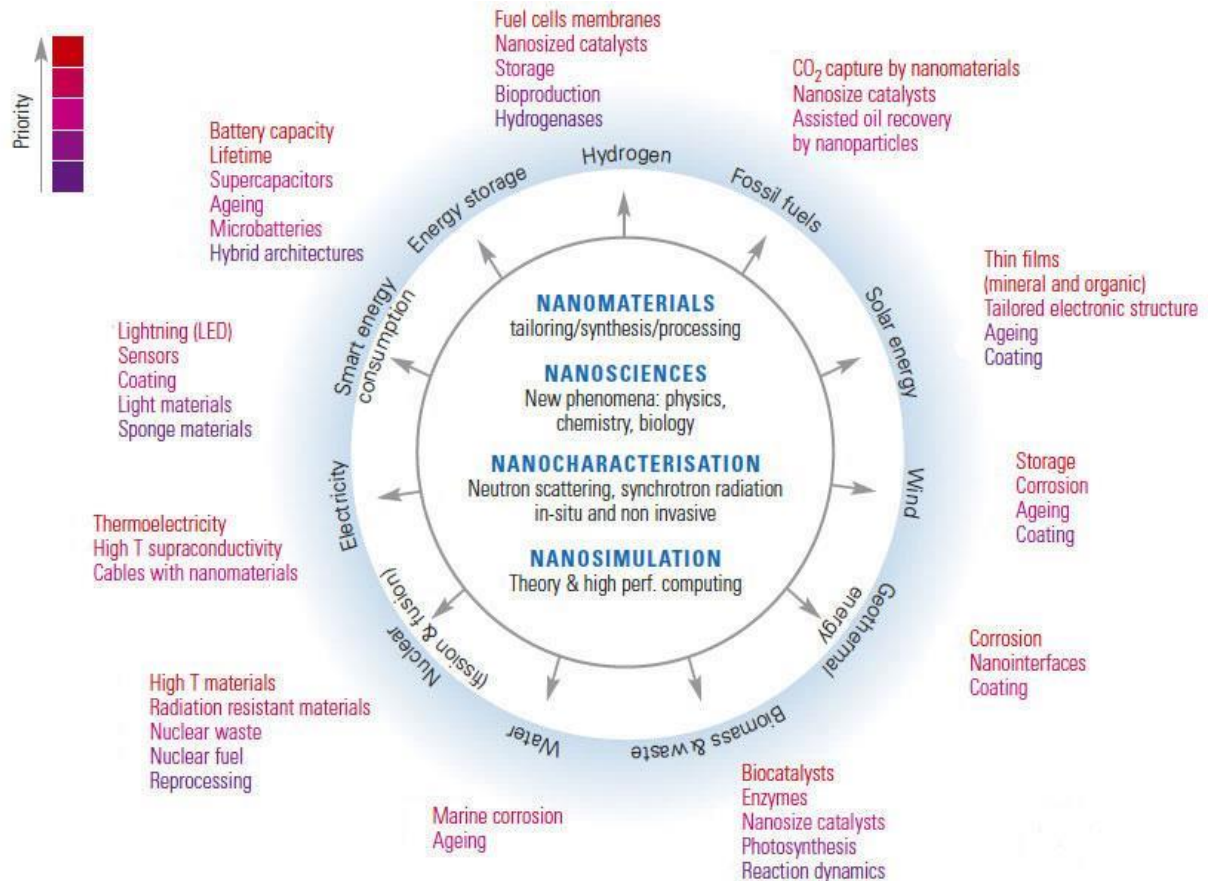
Figure 1.7: Brief overview of nano technology applications

1.9 Superconductivity

Superconductivity of a material is referred to an abrupt decrease in its electrical resistivity down to zero at a certain critical temperature. Above this temperature these materials behaves as normal conductors. Superconductors were firstly observed in 1911 at Leiden University by Dutch physicist Heike Kamerlingh Onnes. The resistance of mercury suddenly disappears when it was cooled to the temperature of liquid helium at 4 degree kelvin (-269C). Below critical temperature, their properties are characterized by two basis effects. First, they don't offer any electrical resistance. Also, a current circulate within the material without ant dissipation of energy. Secondly, during the transition from normal to superconducting state they expels out all of the magnetic field inside them. This field exclusion behavior is known as Meissner effect. [29]

1.9.1 Meissner Effect

This effect was initially demonstrated by Ochsenfeld and Meissner by 1933 as "magnetic exclusion effect" which suggests; if a superconductor is cooled through its transition temperature in a field below than its "Hc" (critical field), the field flux is not "frozen in", as indicated by the perception of Zero resistance and according to the application of Faraday's Law. Rather, it is casted out by that material. In easy words "superconductor is like a prefect diamagnet". This flawless diamagnetism is induced by the super-current within the material while picking up such a surprising dimensions that induces an equally opposite field to each part of the superconductor. So, a screening effect comes into existance that vanishes upon further increases in field above "Hc". Consequently, superconductivity drops and field again starts penetrating into the material. [30]

1.9.2 Trios and incomplete theory

Ordinary theories of physics are inadequate to explore the superconductivity or any quantum theory of solid state could do it until a time comes when three American scientists John Bardeen, Leon Cooper and John Schrieffer composed a theory explaining the superconductivity in 1957. The word "trios" is referred to these researchers and their theory; known as "BCS theory" according to which the electron pairs are formed due to interaction with crystal. These pairs are called "cooper pairs" and it moves through the solid without any opposition. This pair can moves independently without being scattered. Here, the electron interaction energy is weak and these pairs broke up on increasing temperature that is why superconducting behavior is prominent at very low temperature. BCS theory gives no insight to the co existance of such behavior at high temperature superconductivity and above. But the new era in the field of field of superconductors starts in 1986 after the discovery of high temperature superconductors for example $YBa_2Cu_3O_7$ with TC=92K. [31]

1.9.3 Types I and Type II Superconductors

There are number of elements that signify themselves as a superconductors displaying zero resistivity at low temperature and having the characteristics of expelling the magnetic field from their interior. Superconductivity occurs below a certain critical temperature "Tc" and magnetic field "Hc". These are called as type I superconductors. Some of other materials/alloys found to be superconductors with high critical temperatures and fields as well.in superconducting state they can carry higher current densities. They are called as type II superconductors. [32]

1.9.3.1 Types I Superconductors

Such superconductivity usually exists in pure metals. They have certain critical field above which their superconductivity vanishes and a critical temperature to which they are cooled so their resistivity is lost and they behave as a perfect diamagnet. No magnetic field could penetrate inside them in superconducting state. They are also called as "soft superconductors". Sudden disappearance of their superconductivity towards room temperature limits their practical applications. For example Mo (0.93K), Ru (0.5K), Hf (0.1K), Zr (0.546K), Cd (0.56K), In (3.408K), Pb (7.193) etc. [32, 33]

1.9.3.2 Types II Superconductors

Type II superconductors are commonly made from alloys. They are mechanically harder and own higher critical fields. They have applications in high field superconducting magnets. In such superconductors, vortex states occur and they in present in mixed normal and superconducting states. Type II for e.g. NbTi is used to form coil winding for superconducting magnets used in MRI. These superconductors have the ability to switch their states at two different critical fields. Examples are NbTi (10K), NbN (15.7K), Nb_3Sn (18K) etc. [32, 33]

1.9.4 Cooper Pairs

During the transition from normal to the superonducting state, there occurs a condenstaion of electrons into a state with energy less than fermi level. Electron-phonon interections is responsible of such pairs. Experimental evidence of such interaction was provided by isotopic effect at transition temprature. This condensation of electron becomes the basis of BCS theory. It is obvios that if mercury have electronic conduction, then there should be no dependance of critical mass on nuclear mass but its dependance upon isotopic mass was a remarkabkle evidence of of such electron-phonon interaction. (phonon is quantum of lattice vibrtions). The distance of saperation between cooper pairs is called coherence length. [32]
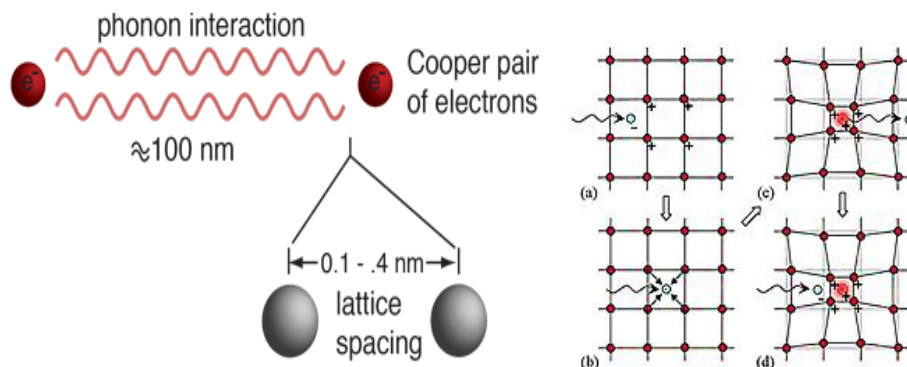
Figure 1.8: Cooper pair of electrons and their phonon Interaction

1.9.5 Existence of critical temperature (T_c), critical magnetic field (H_c) and critical current density (J_c)

Superconductor has three-type of critical point (critical value).

- ❖ Critical Temperature: T_c
- ❖ Critical magnetic field: H_c
- ❖ Critical current density: J_c
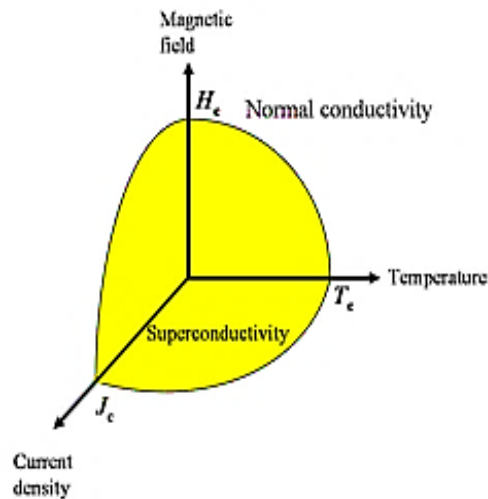
Figure 1.9: Critical Parameters of a Superconductor

1.9.6 Applications of superconductors

Though applications of superconductor are limitless but few of them are given.

- ❖ Superconducting Magnets In MRI/NMR
- ❖ Mass Spectrometer
- ❖ Beam Steering Magnets In Particle Accelerator
- ❖ Plasma Confinement Magnets In TOKAMAKS
- ❖ Josephson Junction (Basic Building Block Of SQUID)
- ❖ Magnetic Levitation Devices & Superconducting Magnetic Refrigeration
- ❖ Smarts Grids & Superconducting Transmission Lines

1.9.7 Nobel prizes in superconductivity

Sr. No.	Year	Nobel Laureates	Contributions
01	1913	Heike K. Onnes	For investigating the low temperature properties of matter, that led to the production of Liquid Helium
02	1972	J. Bardeen, L. cooper, J. Robert	For their Famous BCS theory. The theory of superconductivity
03	1973	L. Esaki, I. Giaever, B. D. Josephson	Experimental discoveries about tunneling in Semi. and superconductors
04	1987	G. Bednorz, Alex Muller	Break-through in discovery of superconductivity In ceramic materials
05	2003	Alexei Abrikosov, L. Ginzburg, A.J. Leggett	Pioneering contributions to the theory of superconductors and Super lattice
06	2016	M. Kosterlitz, D. Haldane, D. Thouless	Theoretical discoveries in Topological phases and phase transitions

Table: 1.1 Nobel prizes in superconductivity [34]

Chapter 02 Literature Review

Our work is mainly focused upon the synthesis of two dimensional transition metal carbides named "MXenes" and their applications in the field of nano magnetism and superconductivity. MXene similar to graphene comes out an outstanding member of two dimensional materials family with its promising properties and applications in various fields of energy storage, biomedical applications, magnetism and electromagnetic shielding. Mxenes are derived from their 3D parent Phases known as "MAX" by wet chemical reduction method of middle "A" layer and finally obtaining hexagonally stacked sheets of "M-X" layers. Scientists are currently working on this recently discovered 2D material and different other MXene phases.

2.1 World's Attraction Towards 2D Materials

The discovery of 2D Graphene material in 2004 by Novoselov et al. attains a huge attention of entire scientific community towards its reliable synthesis methods, different applications and physical properties. It becomes forefront research area in materials sciences and engineering. Moreover, layered structure of BN, WS_2 and MoS_2 and other 2D materials were also integrated from their 3D structure by micromechanical exfoliation and their structure of layers is held together by van der Waals interactions. [35, 36]

2.2 MAX Phases

Currently, more than 60+ different known different early transition metal carbide and/or nitrides MAX phases are present. Most of the MAX phases in powder form known to the date were discovered by Nowotny et al. in 1960s, after that the synthesis of Bulk Ti_3SiC_2 samples by Barosum& El-Raghy and its unusual properties develops an interest in such solids. Then the research on the MAX phases has exploded. [37-39]

2.3 MXene discovery and Production

In 2011, Michael Naguib and his fellows at Drexel University, Philadelphia, USA had discovered a new 2D material known as "MXene". They did it successfully by synthesizing the two dimensional network of MXene sheets through wet chemical etching route of parent 3D MAX phase. Due to structural similarities with Graphene such 2D structure, it was named as Mxenes. MXenes are layered structures of early transition metal carbides and/or Nitrides which are derived from 3D MAX phases (space group P63/mmc) in which "M" is the early transition metal e.g. Ti, Ta, V etc. , "A" is mainly group 13 or group 14 element (group IIIA or IVA) e.g. Si, Al and "X" is the carbide, nitride or can be both and n=1, 2, 3 represents the number of layers, forming 211, 312 and 413 phases. The nature of bonds between M-X layers is mixed ionic, covalent and metallic nature while the bond between M-A layers is just metallic. Due to this difference between relative intensities of the bonds it is feasible to selectively remove the A layer chemically without any disturbing to the MX layers. "A" layers elements are more chemically reactive to the Fluoride containing compounds so etching is done by HF acid.

$$M_{n+1}A X_n + y\,HF = M_{n+1}X_n \quad +AF_y + \frac{y}{2}\,H_2$$
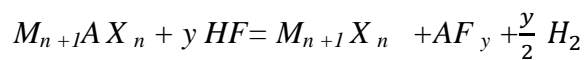
Upon etching the M-X layers are terminated by different surface terminations e.g. O, F, and OH etc. [40-45]
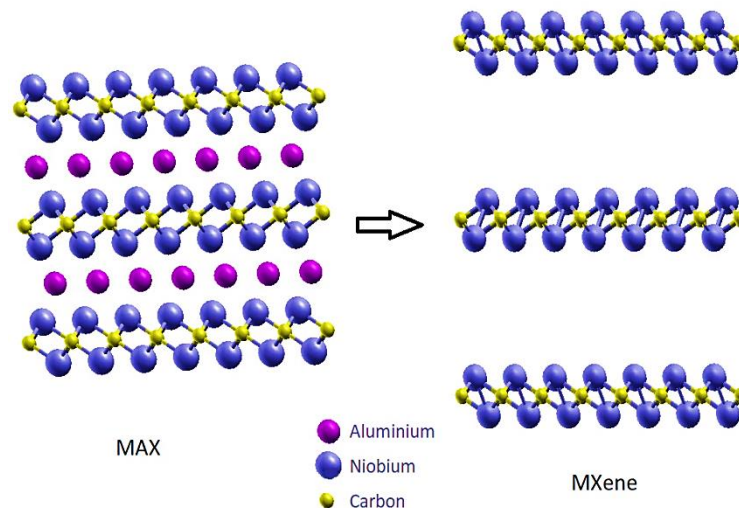
Figure 2.1: Atomic representation of MAX and their Corresponding MXene Phase

Table: 2.1 summery of MAX Phases

413 MAX Phases	312 MAX Phases	211 MAX Phases
Ti_4AlN_3	Ti_3AlC_2	Ti_2CdC, Nb_2SnC, Nb_2PC, Mo_2GaC, Zr_2TlN,
V_4AlC_3	V_3AlC_2	Zr_2SnC, Nb_2AsC, Zr_2SC, Nb_2SC, Hf_2TlC,
Ti_4GaC_3	Ti_3SiC_2	Ta_2AlC, Ta_2GaC, Hf_2PbC, Hf_2SnN, Sc_2InC, ,
Ti_4SiC_3	Ti_3GeC_2	Ti_2SC, Zr_2InC, Zr_2PbC, Ti_2GaC, TI_2InC,
Ti_4GeC_3	Ti_3SnC_2	Ti_2TlC, V_2AlC, Cr_2GaC, Ti_2AlN,Ti_2InN,
Nb_4AlC_3	Ta_3AlC_2	V_2GaC,V_2GaN,Hf_2SnC,Cr_2GaN, Ti_2PbC,
Ta_4AlC_3		V_2GeC, Cr_2AlC, Cr_2GeC, Ti_2GeC, Ti_2SnC,
		V_2PC, Zr_2TlC, Nb_2AlC, Nb_2GaC, Nb_2InC,
		V_2AsC,Hf_2SC

Table: 2.2 Summery of etching Mechanism of different MXenes

Precursor	Etchant	Etching conditions			Loss Weight (%)
		Conc.	Temp.	Time Hrs.	
Ti_2AlC	HF	10wt%	RT	10	40
V_2AlC *(attrition milled powder)	HF	50wt%	RT	8[*]	45
				90	40
Nb_2AlC	HF	50wt%	RT	90	~0
			55°C	40-48	~0
Mo_2Ga_2C	HF	25wt%	55°C	160	NA
	HCl+ LiF	20+1.56	35°C	384	NA
Ti_3AlC_2	HF	50wt% (25w %)	RT	2-24	~0
	HF	25wt%	RT	24	NA
	HF	10wt%	RT	24	NA
	NH₄HF2	10wt%	RT	24	~0
	HCl+ LiF	1M	RT	120	30
		10+0.66	40°C	45	~0
$Zr_3Al_3C_5$	HF	50wt%	RT	72	NA
Ti_3AlCN	HF	30wt%	RT	18	20
Ta_4AlC_3	HF	50wt%	RT	72	10
Nb_4AlC_3	HF	50wt%	RT	96	23
Ti_4AlN_3	HF	20wt%	RT	30	NA

J. Halim et al. (2014) have reported the fabrication of epitaxial thin films by etching the Ti_3AlC_2 in aqueous HF or NH_4HF_2 solution at room temperature before and after etching. This leads to 25% increase in c-parameter (~25Å) when treating with NH_4HF_2 as compared to its value upon treating with HF. It is also observed that both the films exhibit metallic conductivity to 100K temperature. Upon further decrease in temperature, it shows negative trend in its resistivity which increases with decreasing the temperature. It displays negative magnetoresistance (MR) at low enough temperature. Such MXene films could be the promising materials in transparent conductive electrodes, Sensors with some possibilities in order to increase their conductivities etc. [46]

In 2014, Michael et al. reported a different etching technique in order to etch MXene from corresponding MAX phase. Instead of using HF, they use a solution of LiF and HCL. The resultant product was hydrophilic "**clay**" like material and can be dried into a conductive solid and can be rolled into films of minimal thickness also. This additive free MXene clay exhibit exceptional rate performance and cyclability have volumetric capacitance to 900 F/cm^3 or 245 F/g when used as supercapacitors electrode in H_2SO_4 electrolyte. [47]

The use of MXene in Electromagnetic interference (EMI) shielding has been reported in 2016 by Faisal Shahzad and his co-workers. Materials with good flexibility and high conductivity with small thickness are highly demanding in this field. An EMI shielding of 92 decibels by 45μm thick Ti_3C_2Tx film was a successfully achieved which is comparatively higher than other fabricated materials of similar thickness. This comes due to the multiple internal reflections in MXene films and their excellent conductivity (4600 Siemens/cm). Films of thickness from 1 mm to 45mm also provide good electrical conductivity and Electromagnetic shielding. [48]

In 2018, Zhuang, et al. reported a superparamagnetic two dimensional Ti_3C_2 MXene for efficient cancer treatment. They synthesize this MXene with the help of in situ growth of Superparamagnetic iron oxide nanoparticles (IONP's) on the surface of Ti-MXene depending upon definite chemistry of IONP's-Ti_3C_2. This magnetic structure of MXene (IONP's- Ti_3C_2 composite) shows contrast enhanced tumor MRI and high relaxivity of T_2 (394.2 $mM^{-1}s^{-1}$). Such a superparamagnetic MXene found the capability of large photo thermal conversion with 48% efficiency that assure the active photo thermal killing of cancer cells and tumor tissues. This type of high

biocompatibility render the application of as synthesized Iron oxide NP's embedded Mxenes towards future clinical translation e.g. in cancer treatment, theranostics nanomedicine. [49]

2.4 Niobium Based MXene Synthesis and Applications

In 2012, Michael Ghidiu, et al. gives a report on exfoliation of a different two dimensional ternary transition metal carbide and its structural analysis. Room temperature etching of Nb_4AlC_3 (n=3) (<39μm particle size) MAX phase commonly knowns as M_4AX_3 (413-Phase) was done by 48-50 % aqueous hydrofluoric acid for 96h. The etched powder was further centrifuged and washed with water until its pH ~ 5 is reached and collected after drying with 77% yield. Structure was investigated by pair distribution function. XRD Result's demonstrates a significant increase in "c" lattice parameter of the resultant MXene that was attributing to the water physisorbed inside the layers and also indicated by larger O-contents in the energy dispersive X-ray Spectra (EDX). The resistivity of Nb_4AlC_3 MXene comes out to be $4.6×10^{-3}$ Ω.m making it more conductive than other family members with higher "n". [50]

In October 2013, Michael Naguib and his co-workers give a first report on the synthesis and selective etching of new member of MXene's family and its electrochemical activity as an electrode material for lithium ion batteries. The synthesis of Niobium carbide "Nb_2C" MXene was done successfully by selective removal of middle "A" layers from Nb_2AlC leaving a layered MXene behind. Etching was done at different temperatures (RT and 55°C) and time (90hrs and 40hrs) in 50 % HF solution followed by washing and drying of collected powder at room temperature. The HF etching leaves some surface terminations behind like O, OH and F; moreover, some traces of physisorbed water were found in Nb_2CTx layers. The same is the case with Vanadium carbide (V_2CTx) MXene. Upon testing the electrochemical activity of both of the MXenes as an electrode material of lithium ion batteries, it was found that both of these MXenes have their own voltage profiles and have the capacity to functions as electrode material. At lower lithiation voltages, Nb_2CTx shows a reversible capacity of 170 m A·h· g−1 at 1 C while V-MXene exhibit higher capacity. Both have strong capacity to handle high cycling rates (10 C) and efficient Lithium diffusion among the layers suggests their use in High performance applications. [51]

Olha Mashtalir et al. (2015) pointed out a procedure for its delamination using a different organic solvent in place of Dimethyl sulfoxide (DMSO) after the reports on successful exfoliation of the Nb_2C MXene sheets. DMSO was used previously in Delamination of multilayered Ti-MXene flakes. The etched MXene powder was added to aqueous solution of iso-propylamine (i-PrA) in certain ratio followed by 18h stirring at room temperature and washed with DI water. The intercalated Nb_2CT_x was further sonicated for 1h in "Ar" environment to prevent oxidation. Specific quantity of the liquid was filtered by 0.1um size filter and dried in vacuum and fraction of the delaminated MXene was obtained. [52]

Synthesis of Nb_2CT_x-Carbon nano tubes (CNT) films and three different types of three hybrid structures to check their performance to be used in electrochemical energy storage and supercapacitors applications were reported in 2016 by Ayeong Byeon, et al. To prepare Nb_2CT_x- CNT films, the delaminated Nb_2CTx were added in suspension containing CNTs as its final concentration w.r.t to CNTs must be 90% followed by probe sonication of 5 minutes. All these hybrid structure contain exceptional performance as compared to conventional Activated carbon in capacitors electrode. It was observed that Nb_2CT_x- CNT / $LiFePO_4$, lithiated Nb_2CTx-CNT/Nb_2CTx-CNT and lithiated graphite/, Nb_2CTx-CNT provides capacity of 24, 36, 43 mAh/g with the ability to be operated within the gate voltage of 3V while Nb_2CTx-CNT cells contains the ability to reverse its polarity with positive potential 0-3V to negative polarity -3V to 0V, also high volume energy density (50Wh/L, based upon volume of the electrodes) much greater than that of conventional AC capacitor or lithium titanate. It is also reported that the gate voltage of Nb_2CT_x- CNT / $LiFePO_4$ can be further enhanced by using alternate cathode materials e.g. $LiCoO_2$, $LiMn_2O_4$, etc. [53]

In 2016, Single step CO_2 oxidation of two dimensional Nb_2CT_x MXene leads to the formation hierarchical hybrid material of uniformly distributes T-Nb_2O_5 nanoparticles over the surface of Nb_2CT_x sheets is reported by Zhang et al. High capacitance ability of Orthorhombic Niobium pentoxide and its high charging /discharging capability leads to its application of highly conductive layered matrix which minimizes the energy losses and maximizes the energy and power densities. Experimentally, Nb_2CT_x

powder was treated in horizontal tube furnace after being loaded in quartz boat. Evacuating the tube for 1hr with "Ar", its temperature was elevated to 800°C with gradient of 5°C/minutes for 45 minutes.CO_2 was added into the tube for 1h at a rate of 150 sccm , then sample was cooled in the flow of "Ar". The sample was also examined after being treated at different temperature and flow rates. Electrochemical performance of treated MXene shows significant performance in respects of its charging/discharging capability almost 96% after 2000 cycles compared to its initial capacitance. [54]

Han Lin, et al. has reported the fabrication of Nb_2C MXene followed by successive two step exfoliation containing intercalation and delamination of the MXene sheets. For the first time, they reported the MXene as an effective candidate of in vivo photo thermal destruction of tumor tissue grafts in NIRI and NIR-II bio windows. As prepared sheets of Nb_2C are not stable for biocompatible application and they used polyvinylpyrrolidone (PVP 40) so, Nb_2C-PVP was obtained. Such structure is highly effective for tumor cells destruction and show high photo thermal stability. This few layers surface engineered MXene contains distinctive human myeloperoxidase enzyme responsive bio degradability with an activity of 1.1 Uμg−1/500 μg of MXene-PVP sheets, extensive biocompatibility and high competency towards remove tumor in NIRI and NIRII bio windows. [55]

In May 2018, Halim et al. have pointed out a method to introduce point defects and first report of its kind to study the transport mechanism in Nb_2C MXene. Such defects or cluster of vacancies present in the Nb_2C sheet structure can change its physical properties. In one step, they synthesize quaternary solid solution MAX phase ($Nb_{2/3}$ $Sc_{1/3})_2AlC$ containing "Sc" is minority element; second, selective etching of "Al" and "Sc" results in 2D MXene material (2D $Nb_{1.33}C$) with randomly distribute large number of cluster of disordered vacancies and point defects. Transport measurements of Nb_2CT_x films shows an increase in resistivity a low temperature when cooled down from room temperature to 7K and negative Magnetoresistance was observed at 10K was attributed to variable range hopping (VRH) mechanism. [56]

The application of Nb_2C MXene in biomedical application was further investigated by Han Lin, et al. by making it compatible for chemotherapy through the construction of

"Therapeutic mesopores" onto the surface of 2D Nb_2C using sol-gel method by proper controlling its surface chemistry and perfect surface engineering. Nb_2C was selected for its high photo thermal conversion capability (28.6%) in NIRI & NIRII biowindows for upgraded hyperthermia. Mesopores developing agent cetanecyltrimethylammonium chloride was placed in mesopores for affective chemotherapy. This construction of "therapeutic mesopores" carry some distinguish features as therapeutic delivery agent and provide a safe route to chemodrug loading which leads to greater drug loading capacity of about (32.57 %) resulting enhanced therapeutic mesopores activity for tumor eradication. [57]

Mxenes are derived from MAX by fluoride containing acids in a certain molar ratios. Commonly used is hydrofluoric acid (HF) of different concentration depending upon type of MAX phase used. In case of Nb_2C MXene, 50% concentrated aqueous HF is being used but chao peng et al. has reported somewhat different method for its etching. They have used hydrothermal route of its etching with low toxic, easy to use and safe compounds as HF is dangerous to use. $NaBF_4$, HCl was utilized to synthesize hydrothermal etched MXene (h-MXene) at different temperature and times. They found that h-MXene c-lattice parameter was greater than conventional MXene and much uniform structure. Such larger interlayer spacing and large surface (BET surface area) suggest best adsorption capability of methyl orange and methylene blue dyes. [58]

The polarization reversal under the action of electric field has demanding properties in ferroelectric applications as an analogous to ferromagnetic application. The application of ferroelectric materials could be a promising field in using MXene as a precursor to synthesize such 2D ferroelectric crystals. Shaobo Tu, et al. synthesize M-$KNbO_3$ 2D ferroelectric crystal by adding Nb_2C MXene powder in KOH being followed by vigorous stirring at 50°C with adding Sodium dodecyl sulphate (SDS) surfactant. Further, the reaction was carried out by using hydrothermal in a Teflon autoclave at 190°C for 0-48Hrs in self-generated pressure that results in alkalization and oxidation of Nb_2C sheets. Such MXene based ferroelectric crystals have coercive field (≈50 kV cm−1), remnant and saturation polarization of ≈17 and 21 μC cm−2. [59]

Two dimensional transition metal carbides MXenes are the competent members of its family in respect of its applications in energy storage and spintronic devices. Easy to use and less toxic method for etching Nb_2CT_x sheets using LiF +HCl yielding lithium intercalated MXene. Their electronic and optical properties were reported by Joseph Halim et al. The transport measurement of Li-intercalated Nb-MXene Nb_2CT_x-yLi depicts metallic conductivity below 50K; as it resistance increases with decreasing temperature down to 40K is attribute towards three dimensional variable range hopping mechanism (VRH). Nb_2CT_x sheets show more resistivity than Ti-MXene almost two orders of magnitude greater than Ti_2CT_x. [60]

2.5 Transport Properties of Max and MXenes

P. Finkel, et al. has reported the **transport properties** of ternary transition metal carbide Ti_3SiC_2. Various large grain polycrystalline sample of Ti_3SiC_2 were obtained by sintering, hot forging after annealing for 24hrs at high temperature of 1600°C. The temperature dependence resistivity measurement of the samples in a field of 5T in temperature regime of 4-300K shows a surprising typical metallic-like behavior at temperature less than 90K. Magnetoresistance (MR) measurements depicts a quadratic dependence upon H, thus revealing this MAX phase is compensated conductor with n ≈ p which provides a good agreement with Hall Effect results with high charge carrier concentrations. [61]

After a comprehensive study on electronic and transport properties of Ti_3SiC_2, P. Finkel et al. extended their study to its closest member of Ti-Ternary Carbide MAX Phase i.e. Ti_3AlC_2 & Ti_4AlN_3. Their carrier concentration and mobilities, electrical conductivity and magnetotransport properties were studied as a function of temperature in a range from 0K to 300K. Such phase was prepared by mixing Al_4C_3 powders, graphite and titanium at 1400°C for 16hrs at an extreme pressure of 70MPa. Resistivity measurement of Ti_3AlC_2 shows a metallic-like nature down to 80K, and then resistivity drops down linearly with residual resistivity almost 6 times greater than Ti_3SiC_2 thus showing that later former has great defect concentration than later. Moreover, the results of Ti_4AlN_3 can be explained within single band model while the case with Ti_3AlC_2 is more complex and two-band model is sufficient to describe its results. [62]

Once again a study on optical, elastic and electronic properties of $Ti_3Si_{1-x}GeC_2$ was carried out P. Finkel, et al. The samples were prepared by adding TiC, SiC and Ge powder in a proper stoichiometry at 1875K temperature and 172MPa in a vacuum sealed glass tube for 8hrs. Resistivity measurements of the $Ti_3Si_{1-x}GeC_2$ show a metallic-like nature of all of its compositions. Electrical Conductivity, magnetotransport and Hall Effect measurements of all the samples were explained on the basis of two-band model, also it reveals that $Ti_3Si_{1-x}GeC_2$ is compensated conductor in which number electrons are equal to the number of holes i.e. charge carrier density, n =p$\approx 2\times10^{27}$ m^3. [63]

Systematic study on electronic, magnetotransport, electrical conductivity, and thermal properties of MAX Phases M_2AlC i.e. M=Ti, V, Nb, Cr in a temperature region of 5K to 300K was investigated by J. D. Hettinger. Again, the results of all these measurement in all of these MAX phases were consistent with two-band model with their electron concentration and mobilities are equal to that of holes. Interestingly, their temperature dependent resistivities measurement shows their metallic-like nature which comes from large density of states close to Fermi level, that is also consistent with the previously studied compounds of the same family. [64]

After comprehensive studies on transport properties of Ti_2AlC and Ti_3AlC_2, Electrical, Hall Effect and transport studies on another member of MAX family Ti_2SiC has been carried out by T. H. Scabarozi, et al. the resistivity measurements were obtained under 9T as a function of temperature from 2K to 300K. Hot pressing Ti_2SiC powder carried out in vacuum and enveloped in graphite foil placed in a graphite die with heating at 1500°C at 10°C/min for 5hrs. The temperature dependent resistivity measurement shows a metallic like conductivity of the Ti_2SiC down to temperature of ~50K with decreasing effect. Positive and quadratic magnetoresistance effects at all fields and temperature independent negative hall coefficient shows Ti_2SiC is n-type conductor. All these observations are explained on the basics of Two-band Model upon which most of the MAX Phases are studied. [65]

A few years later after the discovery of MXene, the film growth of MXenes on a substrate in addition to its wet chemical etching was successfully done by Joseph Halim et al. DC sputtered films of Ti_3AlC were etched with the help of NH_4HF_2 or

HF. The films were deposited on a carefully cleaned c-axis oriented sapphire, Al_2O_3 (0001) substrate in a preheated deposition chamber for 5 Seconds that leads to the formation of TiC incubation layers followed by Ti_3AlC_2 layers and etching of the deposited films was performed . In order to explore transport properties of the films, RT and MR measurements were performed from 2.5 K to 300K. Ti_3CT_x-films show a metallic like nature from 300K to 100K temperature, upon further decrease in temperature, its resistivity increases below 100K. Such insulating behavior is attributing to weak localization effect typically found in 2D materials. The –ve MR were performed in both regions (when $d\rho/dT < 0$ and $d\rho/dT > 0$) is again consistent with weak localization effect. [66]

Mo_2C MXene has been synthesized by selective removal of "Ga" from its MAX Phase Mo_2Ga_2C instead of single "Ga" layer by using LiF + HCl or HF by Joseph Halim In 2016. After etching, the process of its delamination was carried out to obtain a colloidal solution of delaminated MXene i.e. $d-Mo_2CT_x$. The obtained colloidal solution was filtered on a membrane results in free standing paper of Mo_2C MXene. The resistivity measurement of Mo-films shows a negative trend upon variation of temperature from 300K to 10K thus exhibiting a metallic behavior. Moreover, upon decreasing the temperature to 10K, resistivity increases from 0.6Ω to 124Ω. Moreover, it shows positive magnetos resistance at 10K. Mo_2CT_x shows a semiconductor like behavior at low temperature that corresponds to variable range hopping mechanism, whereas, Ti_3CT_x shows a metallic nature at low temperature that corresponds to weak localization in the similar temperature regime. [67]

Theoretical studies by Hemant Kumar et al. have described the possibility of transport mechanism in Nitride based MXene e.g. $(M_{x+1}AN_x)$ and their tunable magnetism. Density functional theory, first principle simulations and crystal field theory based comprehensive study on Mn_2NT_x reveals the presence of intrinsic magnetism in such nitride structure as well as Ti_2NO_2 and Cr_2NO_2. In addition to it, their theoretical results suggest that their magnetism is tunable; it depends upon the type of termination attached to their surface. Intrinsic half metallicity, robust ferromagnetism, high Curie temperature (1877 to 566 K) and high magnetic moments ($9\mu B$ per unit cell) suggests them a promising candidate for spintronics applications and attracts an interest towards their experimental fabrication. [68]

In detailed study by James Hart (2019) upon the role of surface terminations and intercalants over a range of different MXenes samples after vacuum annealing. They found increases in electrical conductivity after de-functionalization of MXene after annealing. Other interesting fact they found is their transition from metal to insulator or semiconductor like transport i.e. positive to negative dependence of resistance upon temperature. This provide a significant approach towards termination free MXene, Surface and intercalant engineered structure for semiconducting, conducting, topological insulators or magnetism in MXene structure. [69]

2.6 Superconductivity in MAX and MXene Phases

Synthesis of MAX Phases led by Nowotny El-Raghy and his coworkers in 1960 comes out to be a remarkable discovery after the observation of superconductivity in them. A. D. Bortolozo and his company synthesize a new superconducting MAX Phase Nb_2SnC with high transition temperature ~7.8K. Although, there were few reports available on the superconductivity in few transition metal carbides but Nb_2SnC comes out to be a high temperature superconductor. They suggest that Tc of Nb_2SnC mainly depends upon synthesis conditions. Additionally, they reported that Nb_2SnC is a type II superconductor showing zero resistance and diamagnetism below its transition temperature. [70]

In 2006, S. E. Lofland et al. has pointed out superconductivity in "Nb_2AsC" MAX phase. This superconducting MAX Phase has a transition temperature of around 2K. In this family of materials $M_{x+1}AlC_x$, electron phonon interaction is the influencing factor to their heat capacity and resistivity dependence of temperature. They found their theoretical results were consistent with the experimental data with some exceptional electronic properties in Nb_2AsC. [71]

A. D. Bortolozo and his collaborators published a report on the superconductivity of Ti_2InC. This H-phase Ti_2InC has hexagonal layered structure with space group P63/mmc with its structure similar to the one's reported earlier. Resistivity measurement of this H-Phase layered structure shows zero resistance along with diamagnetism below 3.1K and bulk type-II superconductivity mainly depending upon synthesis procedure. [72]

Superconductivity in Nb_2InC has been reported by A. D. Bortolozo at al. X-Ray Diffraction results indicates that the MAX Phase has hexagonal structure with well-defined lattice parameters. Resistivity and magnetic measurements reveals that this MAX Phase is a type-II superconductor with Tc~7.5K with critical field H~90Oe. Nb_2AInC shows diamagnetism below 7.5K. [73]

Epitaxially oriented Nb_2AlC thin films grown on c- (00l) & r-plane (012) sapphire substrate, MgO (111), Si (100) and polycrystalline Al_2O_3. Films were deposited in magnetron sputtering chamber in temperature range 700°C to 1000°C with some deposition rate of ~7nm/min for a time of 8-10 minutes. "a" and "c" parameters of epitaxially c-axis oriented films are 7.746 Å and 5.246 Å. Electrical resistivity measurements of the films designate metallic nature down to temperature ~2K. Further measurement at low temperature indicates the superconductivity in the Nb_2AlC films with Tc~440mK. [74]

Once more, Superconductivity in Ti_2InN has been reported by A. D. Bortolozo at al. X-Ray Diffraction results of powdered Ti_2InN indicates peaks can be with certain prototype phase Cr_2AlC, also this MAX Phase has hexagonal structure with well-defined lattice parameters. Resistivity and magnetic measurements data discloses that this MAX Phase is a type-II superconductor with Tc~7.3K (greater than Ti_2InN, Tc=3.1K) with critical field H~10.8T and typical diamagnetism below transition temperature. [75]

Lu_2SnC has hexagonal layered structure with space group P63/mmc with structure related to Cr_2AlC. The measurement of its physical properties e.g. Temperature dependent resistivity measurement shows that Lu_2SnC is a superconductor below 5.2K, magnetic measurement (M-H Curve) below 1.8K reveals that Lu_2SnC is a type-II superconductor. [76]

Theoretical studies on the superconductivity of MAX Phases based upon Density functional theory was carried out by M. A. Hadi, et al. Theoretical calculation of newly discovered Ti_2GeC reveals its superconductivity at transition temperature (Tc) of around 9.5K. Elastic properties indicate that this superconducting (211) MAX Phase is monotonically stable. [77]

Since the discovery of MXenes in 2011, thin film synthesis of MXene was first reported by Chuan Xu. Mo_2C films were deposited through vapor chemical depositions at 1085°C on a copper foil sitting on Molybdenum foil; in result films of thickness ~100nm were obtained. The resistivity measurements were obtained as a function of thickness ranging from 3.4-8.3 nm in super conducting region. Resistivity of thin layer 3.4 nm shows a negative derivative of resistance (dR/dT<0) disclosing insulating behavior of the sheets, while thick layers indicates metallic behavior with positive change in resistivity (dR/dT>0). [78]

High quality Mo_2C layers grown on Mo/Cu bilayers substrate by chemical vapor deposition exhibits a typical 2D MXene structure. This structure shows superconductivity and enhanced quantum fluctuations below transition temperature which can be also observed in its MR. Sheet resistance as a function of temperature (2K-300K) shows a typical metallic like behavior. At a temperature ~3.4K sheets resistance sharply drops to zero. Taking a close look on the MR measurements below the transition temperature, with low applied field shows oscillations that comes from screening current circulating on triangle-shaped areas on the surface of Mo_2C in circular loops. The observations of negative magnetoresistance in low field and low temperature superconductive region show robust fluctuation of the phase close to superconductor to insulating transition in this system. [79]

First principle study on Mo_2C monolayers based upon Density functional theory with local density approximation, electron phonon interactions were carried out by Jun-Jie Zhang et al. & Jincheng Lei, et al. superconductivity and critical temperature were examined by microscopic study of BSC-theory with electron phonon interactions. Theoretical results predict that Mo_2C monolayers have the characteristics of tunable magnetism and superconductivity depending upon the surface termination attached with a critical temperature range from ~0-13K. They also predicted that Mo_2C (OH)$_2$ is the most stable of all of them with Tc~ 25.5K and Mo_2C terminated with "Br" can have critical temperature of 12K. [80, 81]

Mo_2C layers grown on Mo/Cu bilayers substrate by chemical vapor deposition exhibits a typical 2D stacked layers of MXene with lattice defects in the resultant structure. Superconductivity was observed in the defects induced surface by STS

technique. Uniform and Strong superconductivity has been observed despite the presence of lattice defects in Mo_2C layer lattice. The transition temperature was almost 8.02K experimentally that was best fitted with theoretical results. [82]

2.7 Table of Critical Temperatures of Various Reported Superconductors

Compound Name	Critical Temp. (Tc)	Phases
Nb_2InC	7.5K	MAX
Ti_2InC	3.1K	MAX
Nb_2SnC	7.2K	MAX
Nb_2ASc	2K	MAX
Ti_2InN	7.3K	MAX
MO_2GeC	3K	MAX
Ti_2GeC (Theo. Pred.)	9.5K	MAX
$Nb_2SB_xC_{1-x}$ (x=0-0.6)	4.8K-2.6K	MAX
Lu_2SnC	5.2K	MAX
Nb_2AlC-film	440mK	MAX
MO_2CX_2 (X=O,H,OH) (Theoretical studies)	0K, 12.6K,25.5K	MXene
MO_2C (Films grown by CVD)	3.2K	MXene
MO_2C (Defects induced)	8.02K	MXene

Table 2.3: Nobel Prizes in Superconductivity

Chapter 03 Experimental Synthesis and Introduction to Characterizations

3.1 Synthesis Approaches

There are different methods are used for the synthesis of nano particles depending upon the type of properties required. Two fundamental approaches are given below. [84]

  i)   Top-Down Approach
  ii)   Bottom-Up Approach
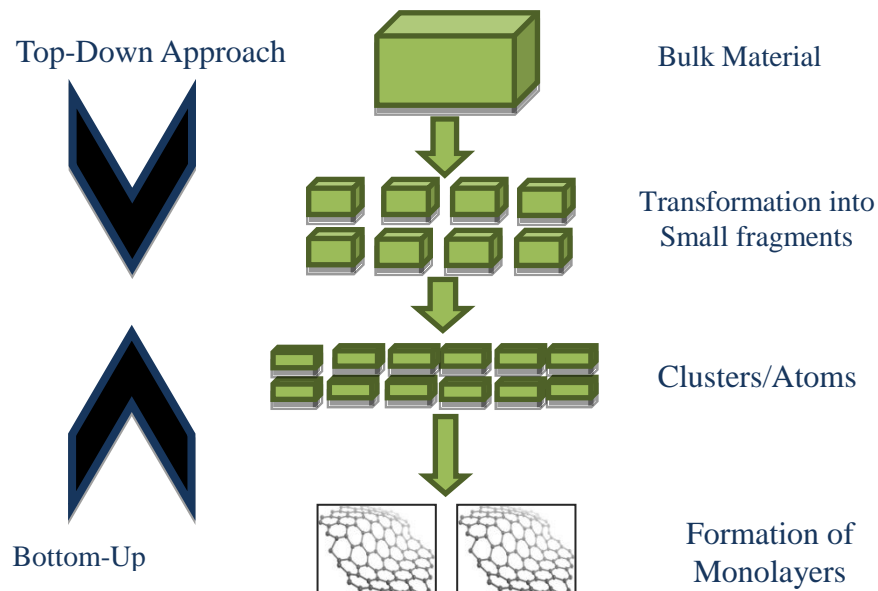
Figure 3.1: Schematics of bottom-Up and Top-Down Approach

I.   Top-Down Approach

As the name of the approach suggests, it is the conversion of a bulk materials to its constituent's particles or the removal of a specific material under controlled circumstances until the required product is formed. Examples are wet chemical etching, ball milling etc. Chemical fabrication methods through Top-down are easy to use and have wide range in industrial applications.

II.   Bottom-Up Approach

Bottom up approach is the formation of nanostructure from miniaturization of components upto atomic level with the procedure of self-assembly. Their construction

can either be atom-to-atom, molecule-to-molecule or clusters-to-clusters. Low temperature synthesis, control stoichiometry and porosity controlled surface area of the assemble structure are the main features of this techniques.

3.2 Synthesis Materials and Tools

These are the following materials and tools are used in order to obtain the MXene from MAX Phase. List of all items is given below.

- Hydrofluoric acid (Sigma-Aldrich 50 wt. % in H_2O, ≥99.99%),
- Niobium Aluminum Carbide (Nb_2AlC) MAX Powder (200 Mesh Size, 95% pure)
- Absolute ethanol (Sigma-Aldrich)
- De-ionized water
- Teflon Autoclave & Petri dishes
- Hot Plate & Teflon coated Magnetic stirrer
- Vacuum drying Oven
- Safety goggles, Gas Mask, acid resistant Gloves

3.3 Synthesis Method

Two dimensional sheets of the MXene were prepared from Nb_2AlC MAX Phase through wet chemical etching route. For this purpose a systematic study of the etching process was carried out at certain range of temperature keeping others parameters constant throughout the scheme. Time, etching temperature and the concentration of the acids used are the main factors to be remembered in synthesizing the MXene. At well optimized time of 30hrs, etching was done at temperatures range of 30°C to 50°C. Took 1g of Nb_2AlC MAX-Powder (200 Mesh Size) and immerse it in 10 ml 48-50% concentrated Hydrofluoric Acid in 1/1 molar ratio in a Teflon autoclave. 10 ml Hydrofluoric acid was poured into Teflon autoclave and placed on pre optimized hot plate for the 15 minutes. Then, MAX powder was added gradually in small amounts in a course of 10 minutes to ovoid over heating of the system because reaction was exothermic. After HF treatment, the resultant powder was washed repeatedly using deionized water in a centrifuge at 2500 rpm until pH reached to ~6. The final powder was removed from foils and left for drying for at 80°C in vacuum oven. Due to extremely harmful nature of hydrofluoric acid (HF), it is compulsory to take all safety

precautions during the reaction by acid resistance gloves, safety goggles and gas mask especially.

3.3.1 Flow chart of etching process

The flow chart describing the detailed etching process is given below,

MAX- Nb2AlC

48-50% HF Acid

continous magnetic stirring for 30hrs at temperature 30°C

after 30hrs, etched power were washed with DI-water several times

Mixed in Ethanol and poured into petri dish

vacuum dried for 24hrs

MXene
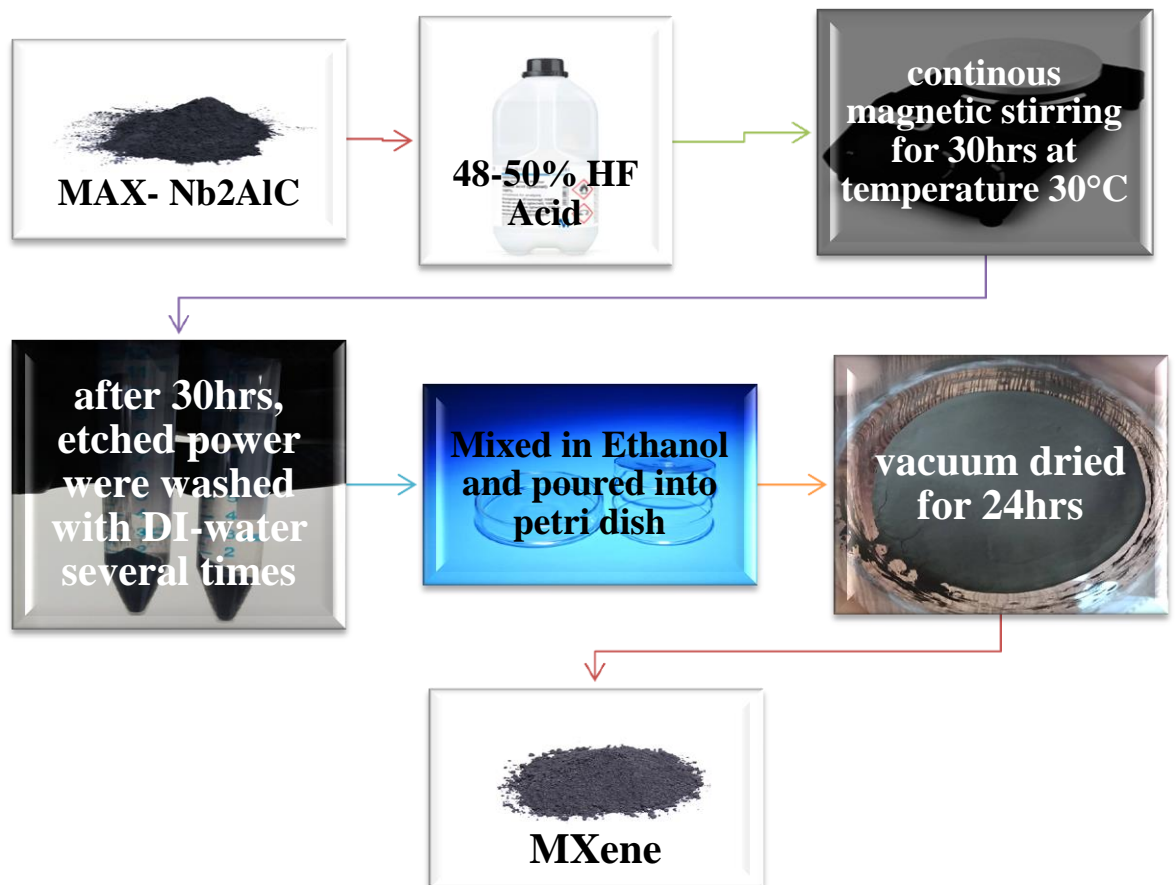
3.3.2 Schematics of Etching Process

Complete etching process can be easily understood by the following schematics.
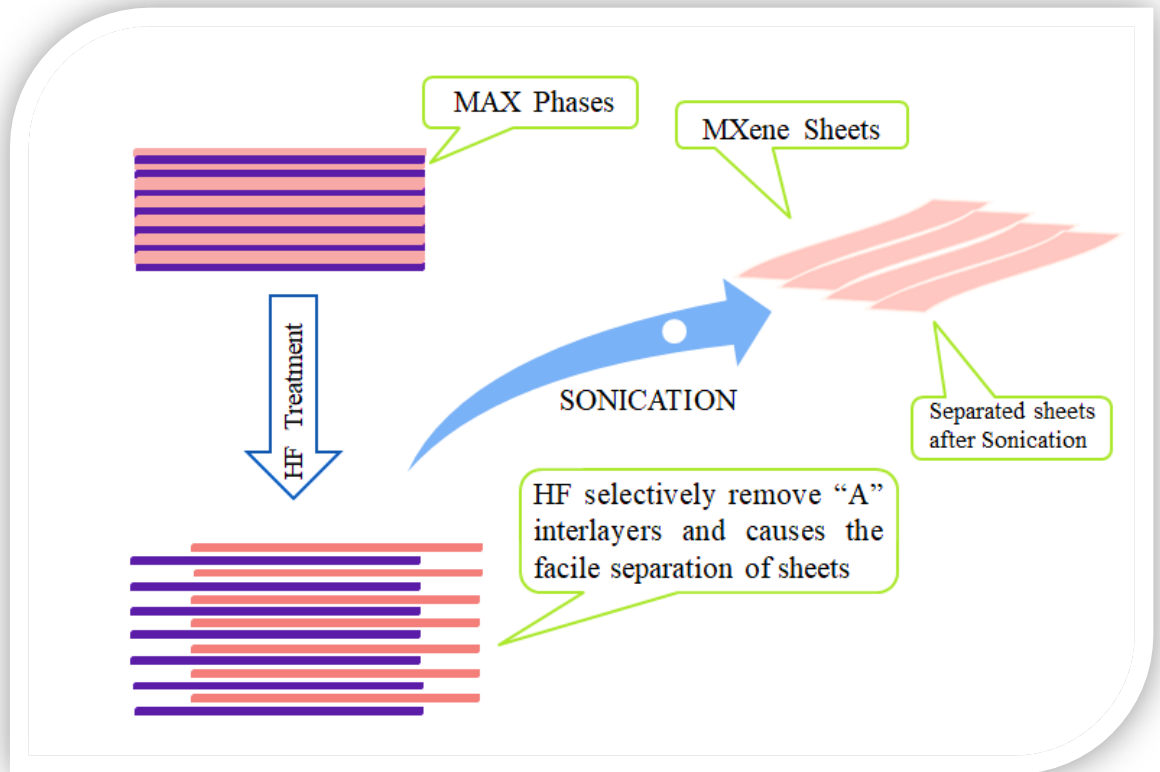
Figure 3.2: Schematic of complete etching process

3.4 Introduction to Characterization Techniques

After synthesis of the MXene powder, the next step is to study their structural, morphological, electrical and electronic properties. For this purpose, following characterizations were utilized.

- X-Ray Diffraction (XRD)
- Scanning Electron Microscopy (SEM)
- Energy dispersive X-Ray Spectroscopy (EDX)
- Raman Spectroscopy
- UV-Visible Spectrometer
- SQUID (Superconducting Quantum Interface Device, MPMS)
- PPMS (Physical Properties Measuring System)

3.4.1 X-Ray Diffraction (XRD)

X-Ray diffraction is a non-destructive technique widely used to analyze powder as well as bulk materials to identify their crystal structure and phase. It is also used to calculate the crystallite size by using Scherrer formula, lattice parameters and other important terms required to study a material.

3.4.1.1 Working principle of X-Ray Diffraction

According to the fundamental knowledge of the optics, when electromagnetic radiations are incident on a plane consist of regular arrangement of obstacles comparable to the wavelength of radiation, diffraction occurs. In solids, there is a regular arrangement of atom, ions and molecules separated by specific interplaner distance in orders of X-Rays wavelength. When X-Ray falls on such atomic lattice, diffraction occurs giving the information about that lattice. This phenomenon is generally used to measure the structure of the material.
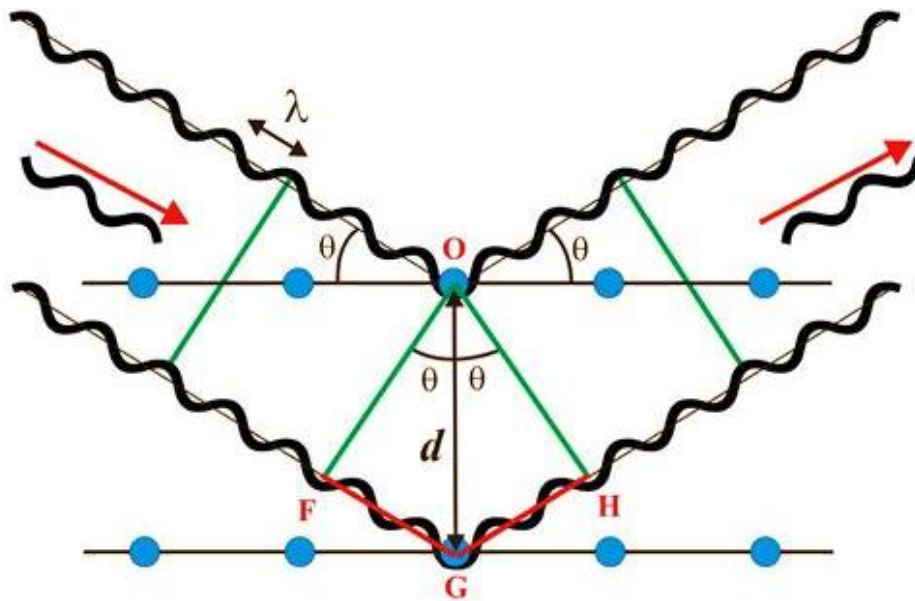
Figure 3.3: Diffraction of X-ray through lattice (Braggs Law) [84]

The process of the diffraction shown in figure 3.3 is well explained by Bragg's law. Bragg's law deals with the diffraction from successive planes of a crystalline structure and provides a fundamental relation between the plane symmetry, incident & diffraction angle and determining the diffraction pattern. As shown in the above schematics, the incident X-Ray is diffracted from two consecutive planes, the path difference is $2d\sin\theta$ which is the integral multiple of the wavelength λ, while d is the interplaner spacing and θ is the angle between incidents and reflected X-rays.

Mathematically;

$$2d\sin\theta = FG + GH$$

$$\mathbf{2d\sin\theta = n\,\lambda} \qquad (\because FG + GH = n\,\lambda = \text{path difference})$$

This is the condition of maximum interference. The above equation is known as Braggs Law Where "n" is the positive integer and represents the numbers of planes. The fundamental principle of this technique in experimental synthesis is the measurement of diffraction intensity as a function of 2θ. Moreover, the particle size from the diffraction can be calculated with this technique by using Scherrer Formula. [85]

$$t = \frac{K\lambda}{A\cos\theta}$$

Where;

t = the mean size of the particles λ = the wavelength of the incident X-rays

K = dimensional Scherrer constant, typical value is 0.9.

A = line broadening at Full width at half maximum

3.4.1.2 X-Rays Generation Phenomenon

The basic principle behind x-rays production is the thermionic emission. In x-ray production high energy electrons produced by heating tungsten filament (copper cathode) are accelerated by high voltage and allowed to fall on a target material (anode). Upon striking the anode, if incident electrons are suddenly decelerated; x-rays produced in these phenomena are called "baking radiations" or "bremsstrahlung radiations". When incident electrons have sufficient energy, inner shells electrons of the target material are knocked out. Such vacancies are filled by upper shells electrons, thus emitting x-rays of energy determined by the electrons energy levels. [86]

38
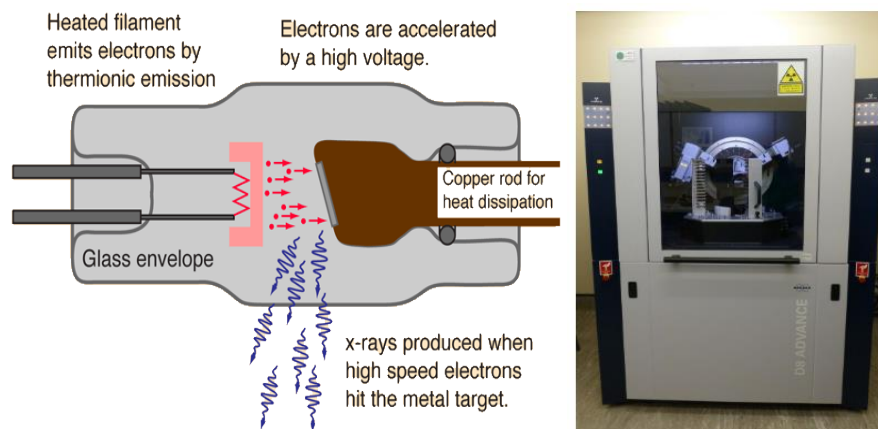
Figure 3.4: X-Rays generation process and X-ray diffractometer

3.4.2 Scanning Electron Microscopy (SEM)

In order to visualize the topographical surface of the sample, the technique of scanning electron microscopy is used which works by scanning the sample surface with high energy incident electrons. SEM is a microscope that uses electrons; it lets you see and detects objects smaller than the wavelength of light itself.

3.4.2.1 Parts inside SEM

- Electron Gun
- Anode
- Condenser lens (Electromagnetic Lens)
- Magnetic Scanning coils
- Specimen stage & Secondary electron detectors

3.4.2.2 Working of SEM

Inside the SEM, there is an electron gun, firing electrons. Coils and lenses direct the incident electron's onto the target. The bouncing electrons are picked up by the detectors and sent to the monitor that builds up the image.
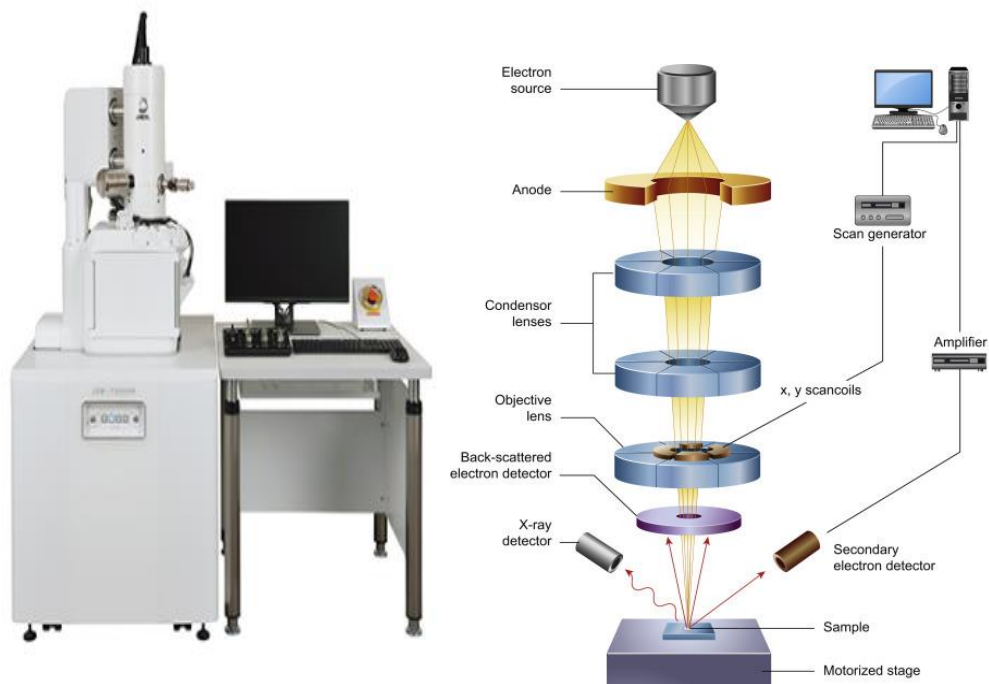
Figure 3.5: Scanning Electron Microscope and its working Phenomenon [87]

3.4.2.3 Sample preparation and safety measures

In order to take images of samples using Scanning electron microscope, the fundamental demand is that the sample would be conducting in nature. There is no problem arises using metallic or conducting samples but insulators creates problem.

To obtain clear images of insulators, a thin film of gold or palladium is coated over the sample to make it conducting. Chemically treated are required to be washed properly and dried thoroughly to avoid destruction of structure due to surface tension [85]

3.4.2.3 Interaction of Incident Electron beam with sample

In details, a scanning electron microscope (SEM) consists of electron source, electromagnetic lenses and electron detectors. It uses an electron beam instead of light bases upon wave particle duality. The electron beam is ejected from the source, accelerated and focused on a sample using the lenses. When primary electrons fall on the sample surface, they lose their energy due to collision and absorption with certain interaction volume in the sample. This interaction generates secondary electrons (SE) and back scattered electrons (BSE). Back scattered electrons results from elastic scattering between incident beam of electron and sample while SE comes from inelastic scattering originating from the atoms inside the samples. Back scattered electron originates form deeper regions and SE from the surface of the sample as shown on figure below.
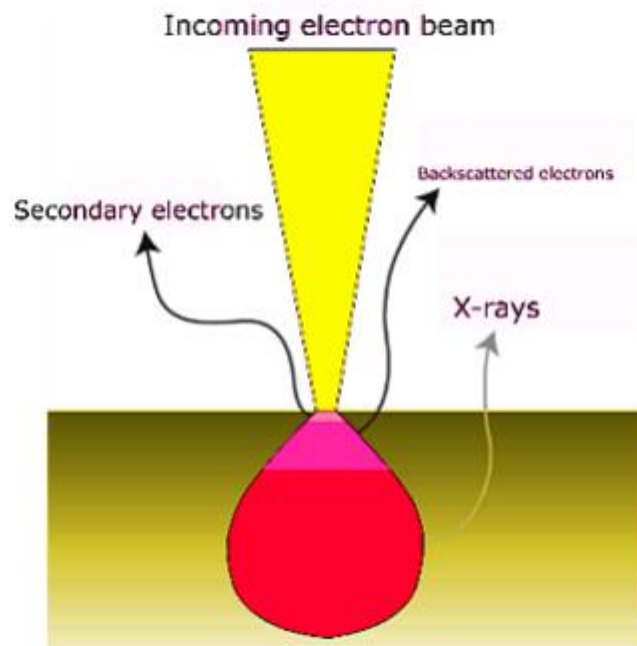
Figure 3.6: the generation of different signals from different regions of the sample [88]

3.4.3 Energy dispersive X-Ray spectroscopy (EDX)

Energy dispersive X-ray spectroscopy is one of the fundamental techniques to analyze the elemental composition. The atomic structure is well studied and it is also known that each element has different compositions and arrangement of electrons inside the

40

atom. Electrons of an atom reside in specific energy levels having distinct energy difference between them. In SEM, X-rays are also produced during interaction of incident beam with sample, also shown in above figure. These x-rays are thus used to determine the elemental compositions. The analysis begins as highly energetic incident beam falls on the samples, penetrates deeply inside the samples knocking out the inner shells electrons of the samples. As a result, a vacancy is created which is filled by any electron available in upper shells of the elements atom emitting an X-ray of specific energy. This specific energy corresponds to certain atomic structure. Hence, the sample's elemental composition can be identified with atomic percentage. [85]

3.4.4 Raman Spectroscopy

Raman spectroscopy is based on an effect known as Raman scattering presented by C.V Raman and K.S. Krishnan in 1982. This spectroscopy is based upon inelastic scattering of incident monochromatic light from the sample. In this spectroscopy, the sample is irradiated by strong laser source in UV-visible region and scattered light is observed at perpendicular direction to the incident beam.

3.4.4.1 Basic components of Raman Spectroscope
There are main parts of a Raman spectroscope given below.

- Laser excitation source
- Excitation delivery optics
- A sample
- Collection optics
- A wavelength separation apparatus
- Detectors
- Recording device

3.4.4.2 Brief View of Scattering Mechanism

When a monochromatic light of frequency "vi" falls on a sample, some part of the light is absorbed and remaining part is transmitted. While, in a direction perpendicular to the sample, a minute part is scattered with some frequency "vf". in first case, the Rayleigh scattering occur at vi=vf where excited electron return back to its initial state. Raman scattering occurs at vi≠vf, this scattering can be thought of two way phenomenon. As electron resides at different vibrational levels, if an electron excited to certain level after absorbing the incident light, it will be de-excited. Here, if electron

falls back to its different levels, it emits a photon of different energy. This gives rise to Raman Stokes and Anti-Stokes Shift. [89]

3.4.4.3 Stokes and Anti-stokes shift

The concept of stokes and anti-stokes shifts is given below through energy levels an atom.
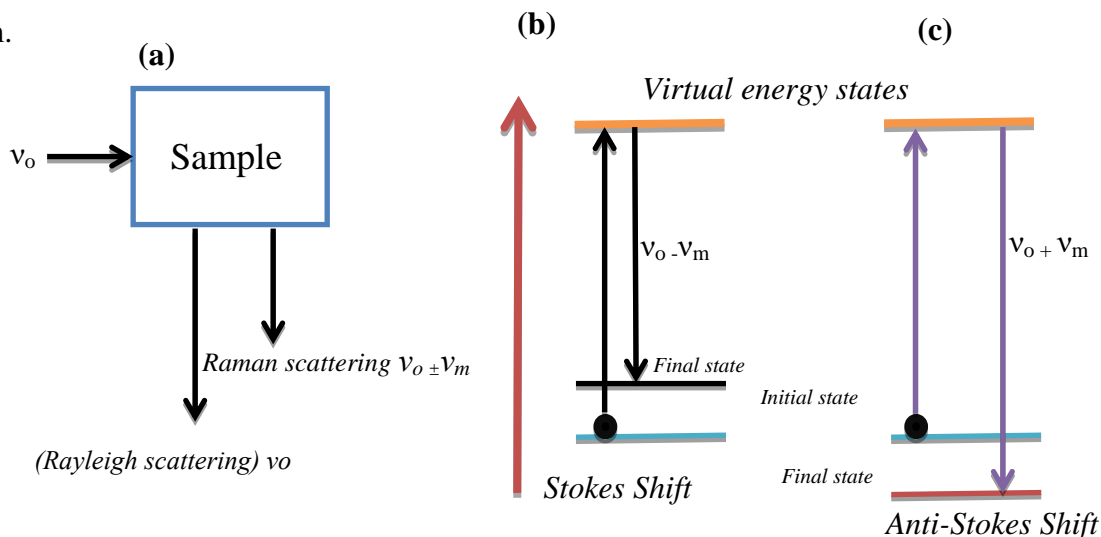
Figure 3.7: Raman scattering energy level diagram (a) Mechanism in Raman Spectroscopy (b) Stokes shift (c) anti stokes shift

3.4.4.5 Wave number and Information gathering

According to encyclopedia Britannica, wave number is the number of waves in a unit distance. It is units of frequency in molecular, nuclear or atomic microscopy which is equal to frequency divided by speed of light. i.e. $K=v/c$. The data provided by scattering in converted into wavenumber and calculation of wave number difference with the incident light is carried out. This difference is given on x-axis while Raman intensity is given on y-axis. In Raman spectrum, peak position indicates the molecular structure, forward/backward shifts in the peaks shows stress in structure, width of the peak shows crystallinity while height of the peak indicates the concentration of substance respectively. [90, 91]

3.4.5 UV-VISIBLE Spectroscopy

UV visible spectroscopy is used to measure the absorbance of light when a sample is focused by visible or ultraviolet light. It is necessary to achieve vacuum condition in spectrometer for measurements. It is absorption spectroscopy and based upon the phenomenon of electronic excitation. In order to understand the working principle of UV spectrometer, Beer-Lambert Law gives an insight that "absorbance of UV light by

the sample is directly proportional to its concentration with its dependence on path length of cuvette." [92]

Mathematically; $A = \epsilon cl$

Where; A = absorbance; c = concentration of solution (mol dm^{-3})

l = optical path length; dimension of the cell or cuvette (cm)

ϵ = molar extinction, which is constant for a particular substance at a particular wavelength (dm^3 mol^{-1} cm^{-1})

3.4.5.1 Working of UV spectrometer

A monochromatic light is focused on a monochromatic .it converts the incident light into single wavelength light. Beam splitter splits the incident lights into two parts, from which one passes through the samples and other one passes through the reference solution. Both of these light beams are recorded after passing through different solutions individually and their difference is calculated which shows that sample beam has less intensity as compared to that of reference solution as it is absorbed by the molecules and there is a greater concentration of molecules in it. [92, 93]
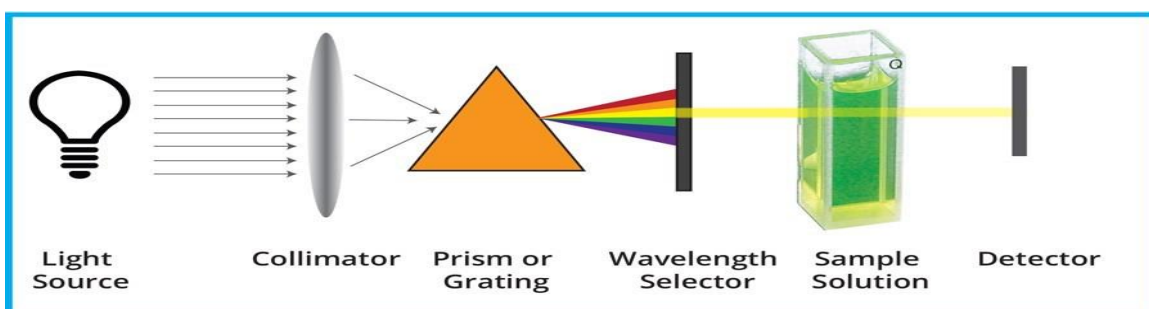
Figure 3.8: a UV-Visible spectrometer Setup

3.4.5.2 Band Gap Measurement

For band gap measurements, tau plot is used

$(\alpha h\upsilon)^n = A (h\upsilon - E_g)$

Whereas, α = Absorbance, A= Proportionality constant; h= Planck's constant; E_g = Band gap energy; υ = Frequency of vibrations;

n= Nature of optical transitions (n=2 direct allowed transition, n=1/2 indirect allowed transitions.

Direct Band gap materials the graph between $h\upsilon$ and $(\alpha h\upsilon)^2$ yields a straight line while in Indirect band gap, a graph between $h\upsilon$ and $(\alpha h\upsilon)^{1/2}$ is obtained. Then straight is line is extended manually to x-axis, where it meets x-axis gives the value of band gap. [94]

3.5 Magnetic Properties Measurement

The magnetic properties measurement involves the magnetic measurements as a function of temperature. It contains Zero field cooling (ZFC) and Field cooling curves (FC) and other magnetic measurements as well. In this work, these measurements were performed by using SQUID and PPMS-9 Quantum design. A detailed discussion of this equipment's is given below.

3.5.1 Superconducting QUantum Interface Device (SQUID)

SQUID is the acronym of superconducting quantum interface device. It consists of two parallel Josephson junctions in which two superconductors are separated by thin insulating layers. This device has the ability to measure extremely small change in magnetic field with the help of these two Josephson Junctions. There are two types of SQUIDS one is rf-SQUID which has only one Josephson junction (superconducting ring is interrupted at one point) and other is DC-SQUID which consist of Josephson Junctions (superconducting ring is interrupted at two points). [92]
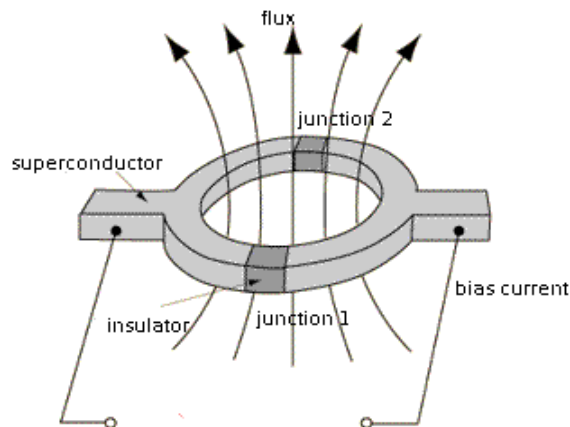
Figure 3.9: Josephson junction in a superconducting loop

3.5.1.1 Josephson junction

It is important to note that devices based upon Josephson have their valuable application in high speed switching circuits. Such devices are manufactured to switch in very small interval of time almost in picoseconds. They also have valuable application in high density computer circuit because of their low dissipation. That is why parallel Josephson junction is used in SQUID to detect very small magnetic fields. In superconductors, the wave function that describes Cooper pairs of electrons is a similar to the wave function of the free particle (exponential like). In the absence of current, all the cooper pairs in a superconductor can be thought of a single wave function with same phase, so can be called a "phase coherent" as by Clarke. As,

44

Josephson junction is made up of two superconducting coils separated by an insulating layer so, cooper pairs experience the process of quantum mechanical tunneling through this insulating layer without breaking their pair. Clarke envisions this tunneling into insulating region, results in interlocking of phase. In results, DC Josephson Effect occurs in which current flow in the absence of applied voltage. [95, 96,97]

3.5.1.2 Working Phenomena of SQUID

Superconducting magnetic coils produce a magnetic field **B** through which the sample is moved slowly at a certain frequency with the help of hydraulic system to be safe from mechanical vibrations. Due to this motion, sample magnetic moment induces a change of magnetic flux in these coils. A superconductor loop is formed that transform a part of this flux from coils into the SQUID. Samples must be moved slowly through these pick up coils to remain in safe slewing rate of circuit. (Slewing rate of an electronic circuit is the rate of change of voltage per unit time). SQUID circuit and input coils have heater that are automatically operated by control module to expel the standing current in the superconducting loops through increasing their temperature above than critical temperature. [98]
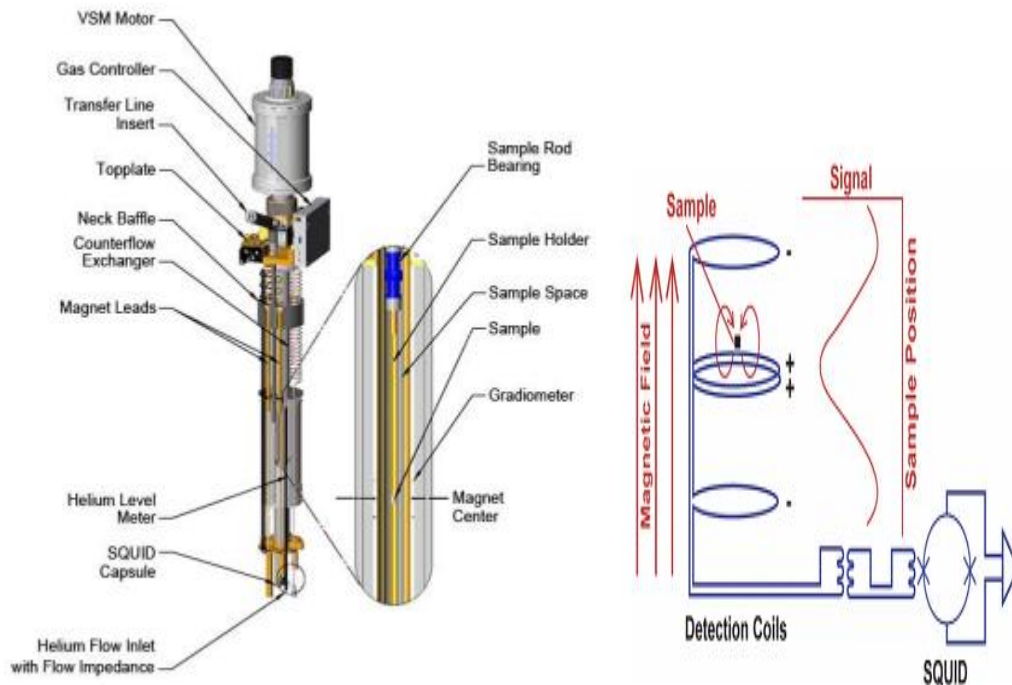
Figure 3.10: (a) SQUID sample holder (b) Schematics of detection [99]

45

3.5.2 Physical Properties Measuring System

Resistivity measurement is the basic measurement through which general and important information about electrical properties of any material can be obtained. The change in the resistivity of the sample with respect to temperature can tells us a lot of information about the nature of the sample and its phase. Especially, performing measurements in the presence of magnetic field aids us to explore the materials properties as a function of applied field. Generally, four or two probe method is used for resistivity measurements in which voltage drop is calculated through inner probes while passing the current through inner probes. Ohms law is used to measure the resistance as V=IR & R=V/I.

3.5.2.1 Biasing/soldering of sample

Silver or indium pastes are used to make electrical contact in a linear geometry for resistivity measurements as shown in figure. Copper wires are connected with silver paste and placed in a samples holder and its wires are connected to measuring instruments. Moreover, Magnetoresistance measurements i.e. the change in resistance of the sample in the presence of magnetic field are performed in the presence of the field. This type of measurements shows significant variation around transition temperatures. [100]
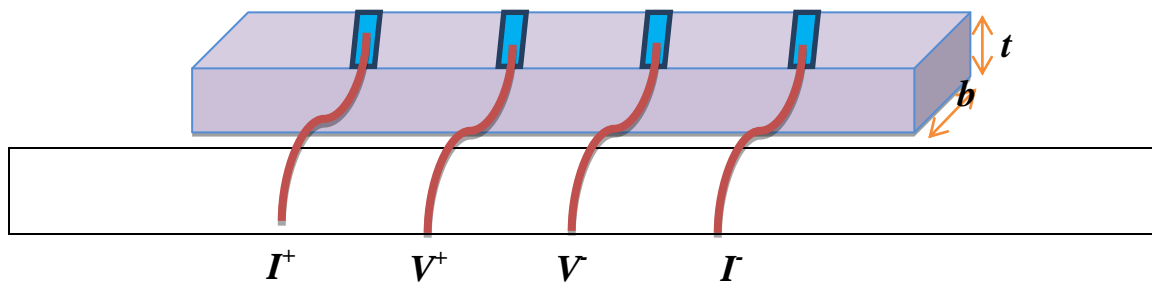
Figure: 3.11: four probe contacts for resistivity measurements

Chapter 04 Results and Discussions

Different characterization techniques were performed in order to analyze the structural, morphological, elemental compositions and magnetic properties of Nb_2AlC MXene powder. The structural analysis were performed by X-ray diffractometer (XRD, Bruker, D8 Advance, Germany) in angle ranging from $2\theta= 5°$ to $70°$. Morphology of the sheets were studied by Field Emission Electron Microscope (FESEM, VEGA3-TSCAN, SEM) at 1µm, 2µm and 5µm resolutions at 20KV respectively along with energy dispersive x-ray spectrum for %age elemental compositions of compound. To explore magnetic properties Magnetization versus temperature (M-T) and Magnetization vs. field (M-H Loops) were carried out by superconducting Quantum Interface device (SQUID, MPMS) at different fields and temperatures.

4.1 Structural Analysis (X-Ray Diffraction Results)

X-ray diffraction results of Nb_2AlC-MAX and layered MXenes Phase etched at different temperatures is given below.
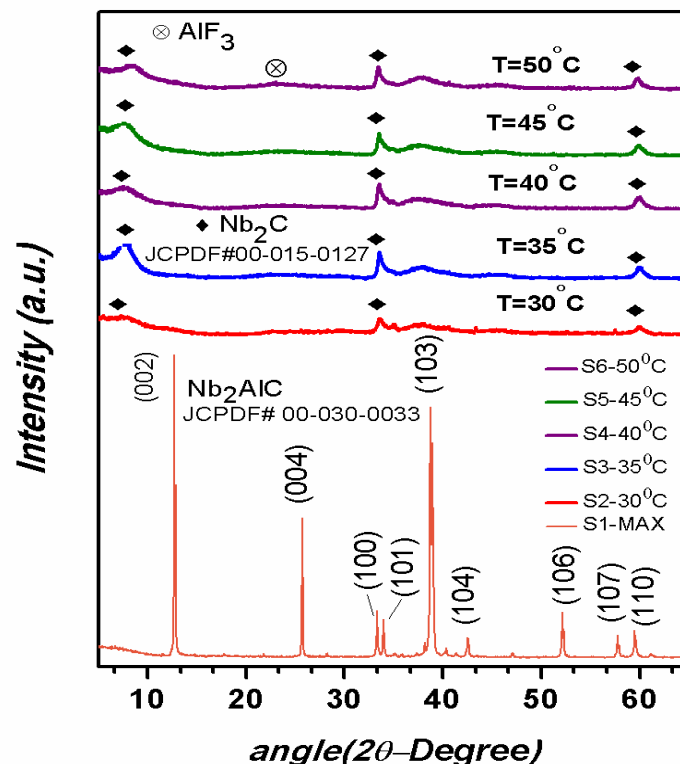
Figure 4.1: (XRD) X-Ray diffraction Pattern of S1-MAX and (S2-S6) MXene etched at different temperatures

In experimental section, systematic study was discussed. As attempts to synthesize MXene at room temperature was not successful, so etching was done at different temperatures for certain optimized time. This gives valuable information about etching temperature required to synthesize this MXene phase. The XRD pattern of (sample-1) pure MAX (Reference code: 00-030-0033) is shown above in figure 4.1. It is important to note that the one major peak in the MAX-Phase is (002) plane that designates the separation of sheets and increase in "c" lattice parameter and other is (103) plane that stipulate the existance of "Al" in MAX. Upon HF treatment peak at $2\theta=12.9°$ significantly reduces and downshifted to lower values $2\theta=7.8°$ which corresponds to the increase in c-LP from 12.8Å (MAX Phase) to 22.72Å (MXene). The variation c-LP is shown in figure 4.2 (b). Due to different relative bond strength between metal-aluminuim and metal-carbide layers, aluminuim is etched out with prominent separation of sheets. While, the peak at 38.9° disappears, shows the removal of "Al" suggesting the complete conversion of MAX to MXene. [51]

Moreover, the sample treated at high temperature indicated the presence of AlF_3 that results due to reaction of HF with "Al" forming Al-flouride salt that remains there dua to incomplete washing possibly. Peaks at $2\theta = 33.4^0$ and $2\theta= 59.8^0$ manifests Nb_2C presence (JCPDS PDF # 00-015-0127). There is decrease in peaks sharpness and cystallity at different peaks that shows the structural losses due to removal of aluminium.
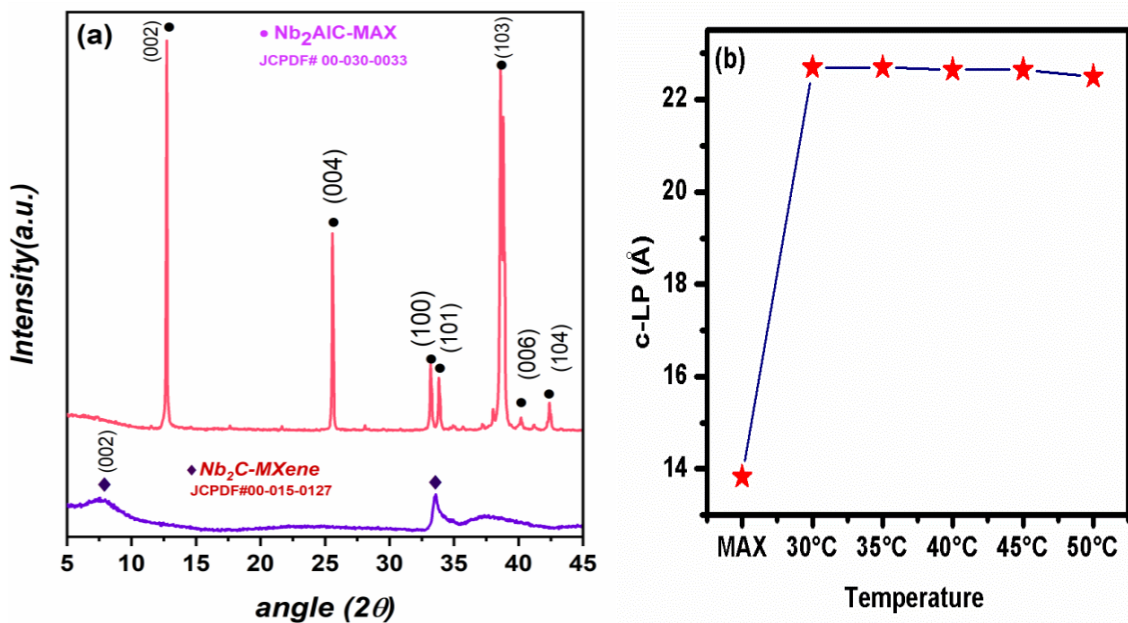
Figure 4.2: (a) XRD of MAX and MXene (b) c-LP Variation from MAX to S1-S6 treated at different temperature

4.2 Scanning Electron Microscopy- structural Morphology
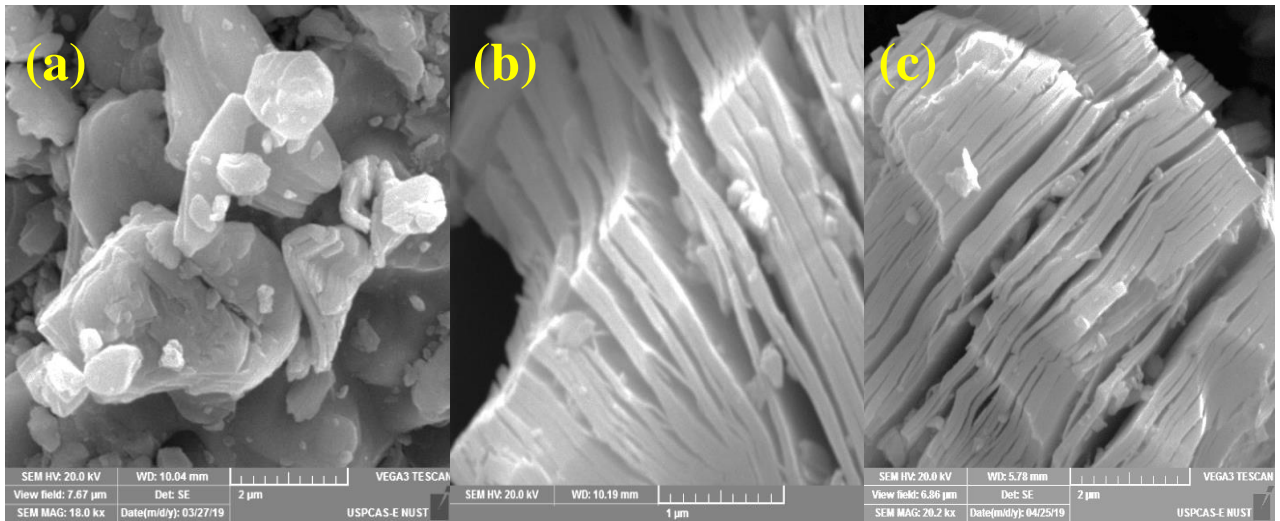
Figure 4.3: Scanning Electron Microscopy Images of (a) Nb_2AlC MAX (b, c) Nb_2C-MXene

at 1µm and 2µm respectively

SEM images of pure MAX and MXene are shown in figure 4.3. SEM images (a, b) of MAX shows that Nb_2AlC is a dense layered solid in which sheets are densely packed. Chemical treating with HF at certain temperature leaves a distinguished lamellar structure of Nb_2C stacked sheets. (Consult schematics in figure 3.2). The removal of "Al" allows the facile separation of sheets that result in clean and well exfoliated accordion like geometry of MXene. The bonds in MAX have the mixture of ionic/covalent/metallic nature; the alteration of strong bonds between M-Al layers by much weaker H-bonds after HF treatment and insinuated water during washing process. Due to difference in relative potency of the bonds between M-A and MC layers permits the removal of interlayers without affecting M-C layers. [51]

4.3 Energy dispersive X-Ray Spectroscopy (EDX)

Figure 4.3 shows the EDX spectra of both MAX and MXene. On comparing the EDX spectra, it is observed that the peak intensity of "Al" in MAX is significantly reduced in MXene. The presence of some amount of "Al" in MXene may be due to Al-fluoride salt. MXene EDX spectra also signatures the presence of "F" that comes from the existance of surface terminations that are unavoidable during wet chemical HF etching MAX phases. Moreover, Oxygen content attributes the presence of water between the sheets as water gets insinuated between the sheets during washing. Peak in both the

graphs give a more significant comparison upon reduction of elemental compositions of the parent (MAX) and daughter phases (MXene).
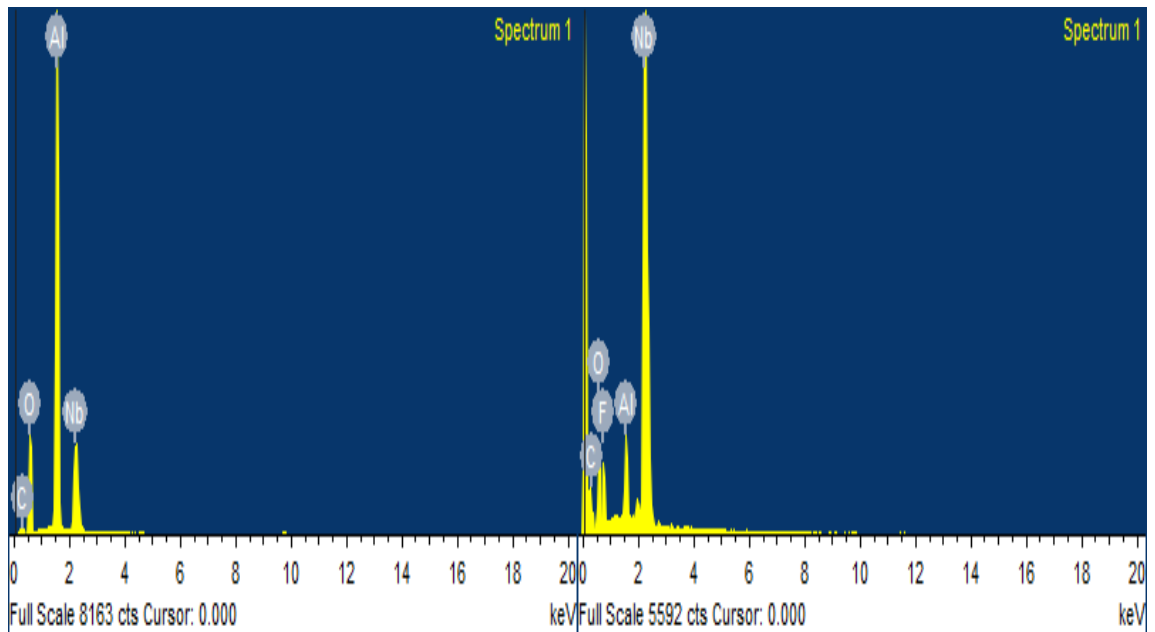
Figure 4.4: EDX Spectrum of (a) MAX (b) MXene (c) comparison of atomic percentage in MAX and MXene

4.4 Raman Spectroscopy

Raman spectra were measured with Horiba Scientific, Xplora. Raman analyzer with laser wavelength 532nm in region 200-2500cm-1.Fig (1) shows the Raman of Nb_2AlC before and after HF treatment at various temperature and conditions. Maximum number of peaks are downshifted, broadened and shifted to higher wavenumber which indicate strengthening of the bond between atoms of MC-layers. This strengthening could be attributing to the presence of some surface functionalization. [101-104]

Peaks I and II suppressed after HF etching, indicating the removal of "Al" layer removal or exchange of "Al" atoms with lighter atoms. Peak III broadened and downshifted so these are related to C atoms. Peaks IV and V gives the signatures about the presence of D and G bands which are actually related carbon species. The D-band characterizes carbon disorder structure to sp3 hybrid carbon and G is graphitic band or sp2 carbon. The ratio of their intensity I_D/I_G tells us about the crystallinity defects. The Intensity ratio of MXene is less than MAX so our structure is more ordered [105-108]
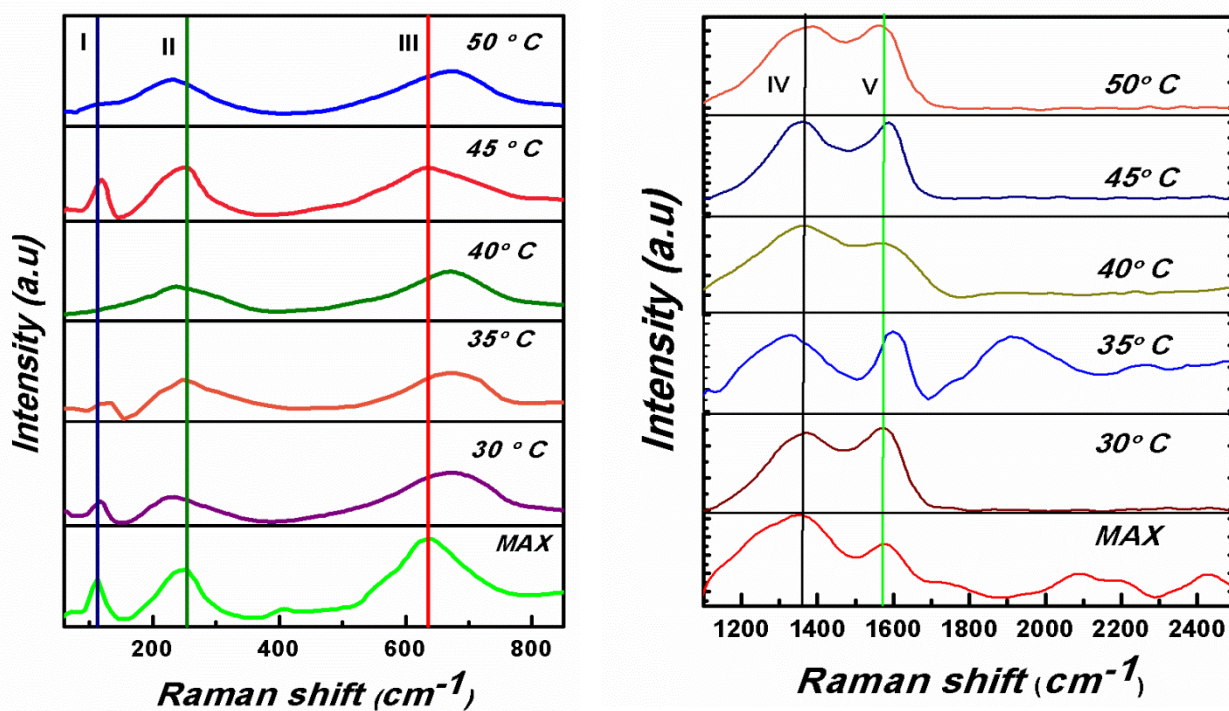
Figure 4.5: Raman Spectrum of (a) MAX (b) MXene treated at different temperatures,

indicating the presence of less defects in MXene (right)

4.5 UV-Visible (UV-VIS.) Spectroscopy

The band gap measurements of powdered MAX and MXene are shown in figure 4.6. The band gap of both were calculated by plotting the graph between $(\alpha h\nu)^2$ v/s (Eg) with a straight line drawn towards X-axis tangent to the graph. The coincidence of this line at X-axis gives the band gap of the both. The band gap of MXene is 1.47ev showing its semiconducting nature at room temperature which can be attributed to the presence of surface terminations.
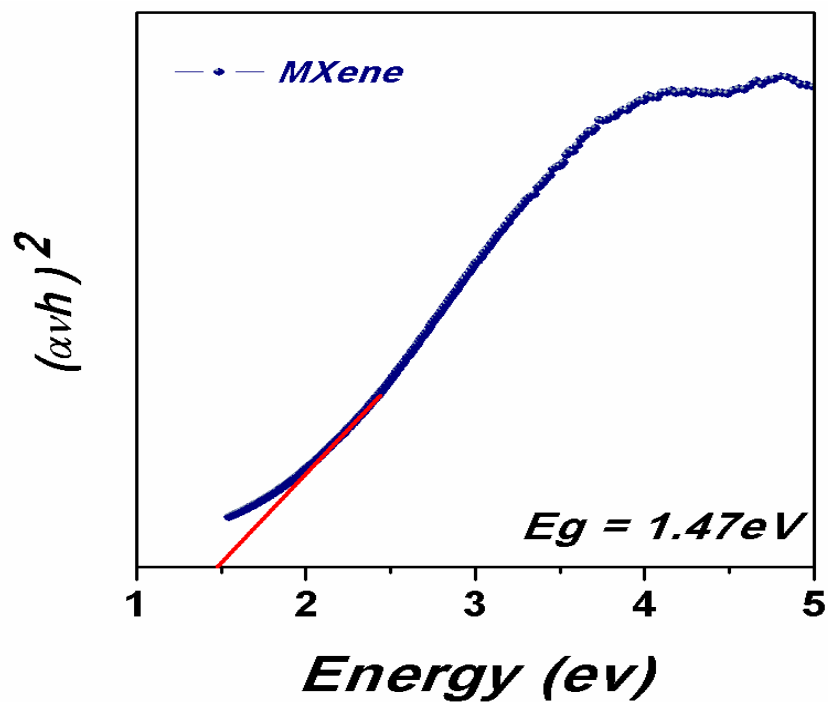
Figure 4.6: UV-Visible Spectra of MXene

4.6 Magnetic Measurements

In order to explore the magnetic nature of the MXene powder, magnetic measurements were performed by using SQUID (Quantum Design, MPMS). The results obtained from these measurements are described below. Due to powder nature of the sample it was difficult to measure transport properties because grains may be discontinuous to provide actual results. During the pellet formation, it is challenging to retain 2D structure inside the sample. So, as-prepared powder was used for magnetic measurements. Before measurements, the powder was put inside a capsule and placed in a tube. Before taking the measurements, this system was calibrated by using oscillatory field in order to eliminate any vagrant field among the coil of SQUID in order to record the real behavior of the powder.

4.6.1 Zero-field-cooled (ZFC) and Field-Cooled (FC) Measurements

Field cooled (FC) and zero field cooled (ZFC) measurements were performed at different field intensities of 10mT and 5mT as represented in figure 4.5 a. it can be observed clearly that at a certain temperature there is transition in both ZFC-FC curves. Furthermore, after this certain value of temperature both these curve starts separating from each other. The value of temperature at which ZFF-FC Curves are merged into each other is onset Transition temperature, noted as T_C^{onset} (K). There is a sharp diamagnetic transition superconducting state. This transition can be observed more clearly in the inset of figure 4.7(a). This superconducting transition from normal state shows a difference between the curves. This difference between ZFC-FC curves is attributed to the fact that in field cooled conditions there is a large flux pinning forces in the MXene-powder resulting in strong trapping of magnetic flux. [109]

Also, there is a presence of some substantial mixed state (vortex state) during transition from positive to negative magnetization for both ZFC-FC curves at each field intensity can be observed at T_C^{onset} (K)≈12.5K, indicating the superconductivity in our sample. This onset temperature T_C^{onset} (K) ≈12.5K, shows the transition of the sample from normal to from normal to superconducting state. Such vortex states start building up just after T_C^{onset} (K) results in gradual decrease in the magnetization of the material. Such vortex state induced superconducting diamagnetism due to super currents that generates a field just opposite to applied field, hence expelling out entire field from their interior and material becomes superconductor. These behaviors suggest type-II superconductivity in our Nb_2C-MXene powder. Also, the width of

temperature signifies the formation of vortex states which confirms type-II superconductivity. [110,111]
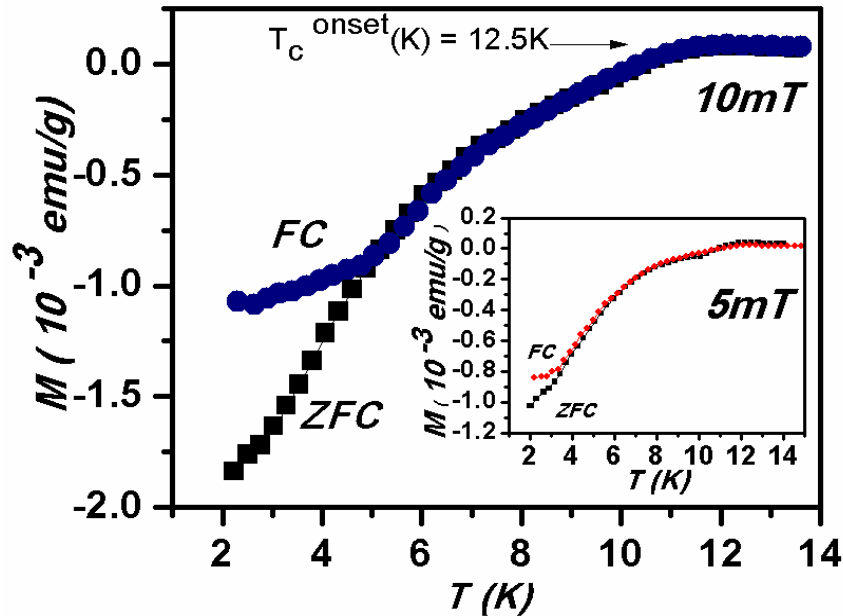
Figure 4.7: (a) ZFC (Zero field cooled) and FC (Field cooled) measurements at 10mT indicating T_C^{onset} (K) with inset at 5mT

4.6.2 Magnetization versus Field Measurement (M vs. H Loops)

To explore more about magnetic behavior of MXene, magnetization v/s field measurements were performed at 5K, 10K and 20K at field range of ± 200mT as shown in figure below. At lower temperature, MH-Loops are similar to the characteristics curves of type-II superconductors. It can be noted that the width of the MH-Loop is different at different temperatures. The width of MH-Loop at 5K is larger than at other temperatures which can be attributed to the presence of strong superconducting diamagnetism in Nb_2C and improved connectivity among the grains. It can be assumed that the sample is losing its superconductivity upon increasing the temperature being consistent with the MT measurements. Vortex formation occurs after transition from normal to superconducting state and getting stronger upon further decrease in temperature, thus inducing strong superconducting diamagnetism. That's why the width of MH-Loop at low temperature is getting wider. Additionally, the vortices are stationary at low temperature and no energy dissipation occurs. Better connectivity results in strong flux pinning among the grain that give rise to strong

superconductivity. While, the increase in temperature disturbs the vortices dynamics, thus disturbing the grains connectivity and weakens the flux pinning among them. So, the material comes to its normal paramagnetic state. This is again consistent with ZFC-FC results that after certain temperature the material is transforming itself into normal state. Thus, increase in vortex dynamics from low to high temperatures results in reduction of flux pinning and superconducting diamagnetic effect among the grains results in reduction of loop width and transition of Nb_2C-MXene Powder to its normal state. The effect of increasing temperature can also be observed in the inset of figure which clearly indicates the loss of superconductivity and transition to normal state upon increasing in temperature. At 12K it gives a straight line which shows the normal nature of the MXene around T_C^{onset} (K) which satisfies the transition depicted by ZFC/FC curves. [112,113]
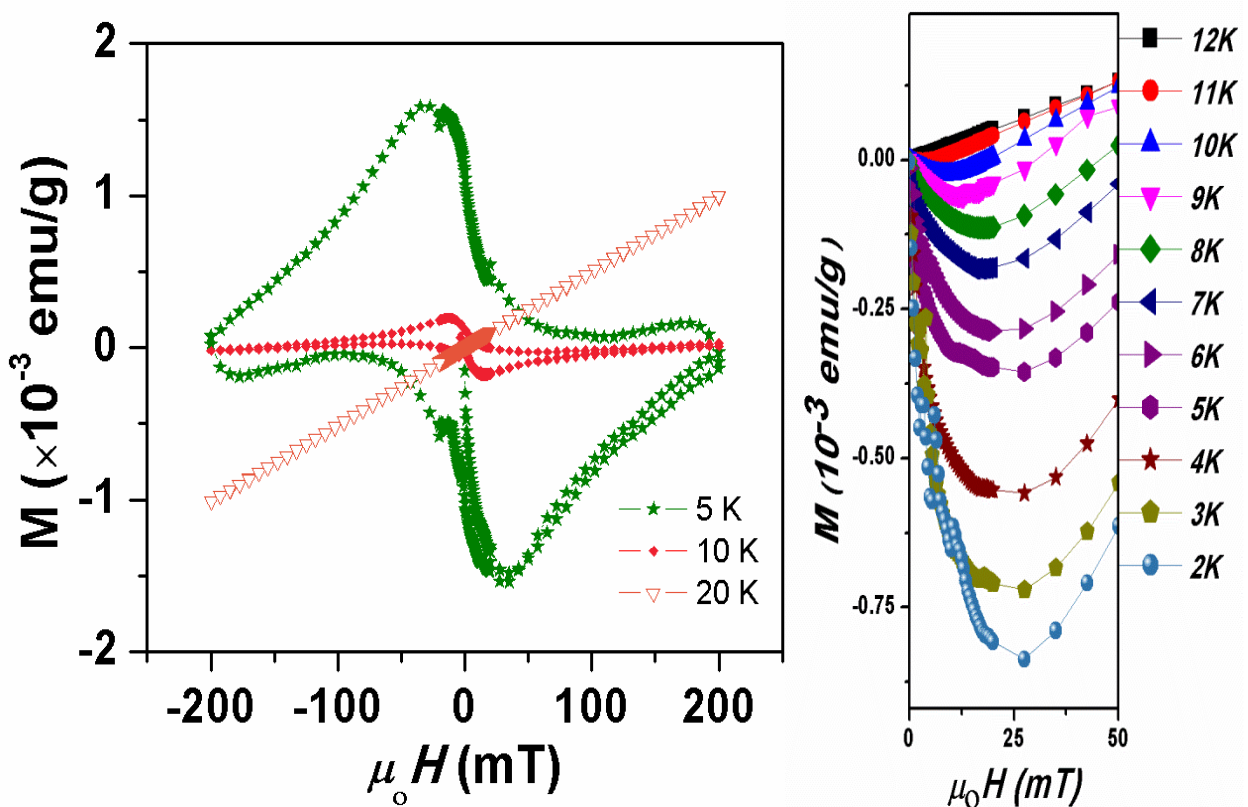
Figure 4.8: MH-Loops (Magnetization vs. Field) indicates typical curves of Type-II superconductors, inset shows a clear picture of Phase transition

4.6.3 Upper (H_{C2}) and lower (H_{C1}) critical Fields and Ginzburg-Landau (GL) Theory Fittings

Upper ($\mathbf{H}_{C2}$) and lower critical ($\mathbf{H}_{C1}$) fields were calculated by quarter curves from zero to maximum positive fields at different temperature as shown figure 4.9 (a) . The variation of magnetization with applied field is recorded terms in $\mathbf{H}_{C1}$ and $\mathbf{H}_{C2}$. Both the fields are monotonically decreasing with increase in temperature. Being consistent with MH-Loop, the splitting between $\mathbf{H}_{C1}$ and $\mathbf{H}_{C2}$ at lower temperature is more prominent. Further increase in temperature reduces the splitting which vanishes at high temperature. The variation of Hc1 and Hc2 as a function of normalized temperature T/Tc is shown in figure 4.6(b). The experimentally calculated values from figure 4.6 (a) are fitted to Ginzburg-Landau (GL) Theory with $Hc_1(T) = Hc_1(0)[1-(T/T_c)^2]$ and $Hc_2(T) = Hc2(0)[1-(T/T_c)^2]$, respectively. It can be seen clearly that experimental data is well fitted with theoretical studies thus satisfying our experimental results and phase diagram in figure 4.6 (b) translates the behavior of type-II superconductors with normal, mixed (vortex) phase and Superconducting state. [113]
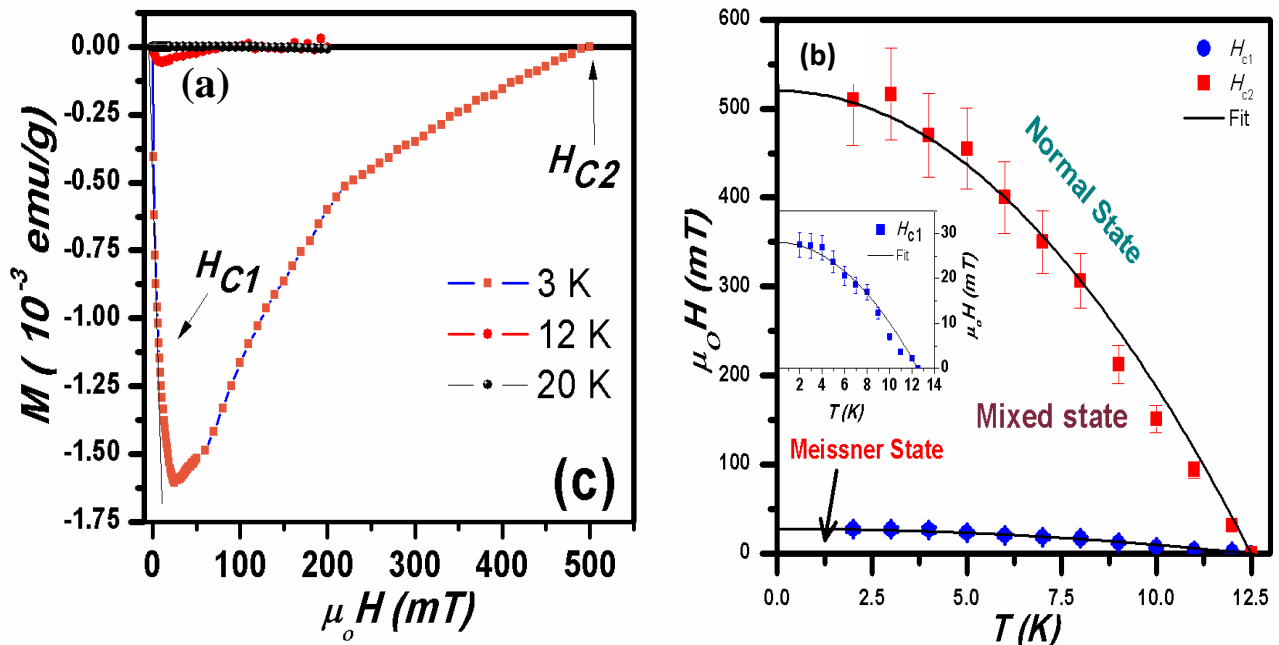
Figure 4.9: (a) Typical characteristics lower (H_{C1}) and upper critical (H_{C2}) fields of type-II superconductors (b) Ginzburg-Landau (GL) theory fittings of lower and upper critical fields represents type-II superconductor's behaviors

4.6.4 Coherence Length (ξ_s) and Critical Current Density (J_C)

Coherence length is one of the important characteristic lengths of a superconductor. It is represented by Greek letter (ξ: *Xi*). It is related to the fact that superconducting electron density didn't change abruptly, rather there a minimum length by which a certain change occurs in a limits so that superconductivity is not destroyed. This minimum length corresponds to coherence length. [114]

Superconducting coherence length comes out to be 25nm was calculated by using Ginzburg-Landau expression $Hc2(0)=\varphi_0/2\pi\xi s^2$, where, φ_0 = flux quantum and $Hc_2(0)$ is estimated with extrapolation of data presented in figure 4.9 (a) which is different than reported one in Mo_2C.

Critical current density (Jc) is important parameter in superconductors in terms of current flow (super current). Bean's Model was used to estimate the critical current density at 5K and 10K, respectively. According to Bean's model: $Jc = 30\frac{\Delta M}{d}$; Here, $\Delta M = [|M+|-|M-|]$ measured in emu/cm^3, d = diameter of the cylinder in cm. As, the dimension of sample are same, so, Jc is directly proportional to ΔM (i.e. width of the M (H) loop). Both the curve suggests that there is a decrease current density with increase in temperature which is in good agreement with ZFC-FC and MH measurement w.r.t to their behavior upon increasing field.
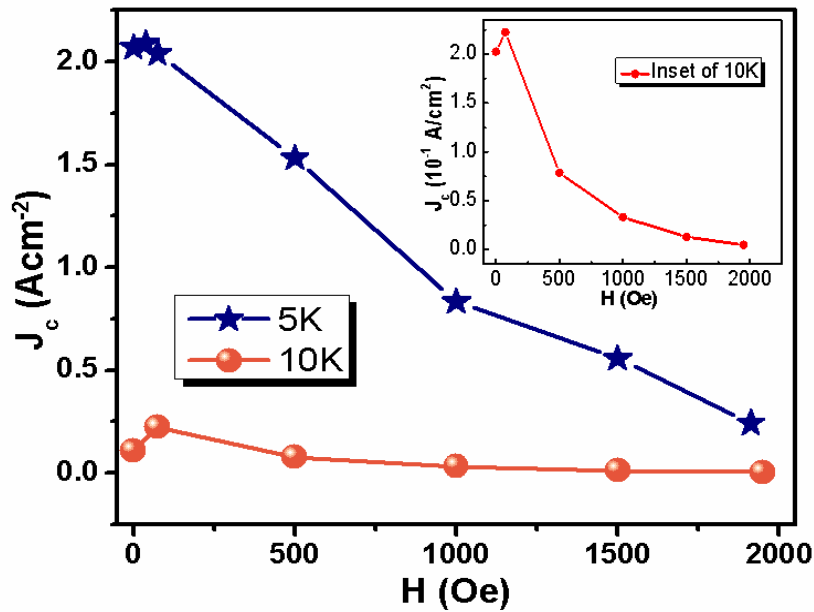
Figure 4.10: Critical Current densities *(Jc)* decreasing with increasing temperature from 5K to 10K

The high value of Jc at low temperature or increase in Jc with decreasing temperature. This indicates the presence of strong flux pinning at low temperatures. There is a decrease in this flux pinning upon increasing the temperature due to increase in vortex motion which leads to a slump in flux configuration and cause energy dissipation in sample. So, enhanced vortex dynamics disturbs the flux pinning and energy dissipation at elevated temperatures results a decreased of Infield Current density values. [115-118]

4.7 Discussion

Now, discussing about the observation of high Tc might be due to the presence of any impurity phase in our sample. Such impurity phases may contain Nb_2C (3D) which has Tc=9.18K or Nb (9.2K), Nb_2AlC (0.44K) or NbC (1.2K). Superconductivity is also reported in Nb_2C (hexagonal 3D, c-LP = 4.9Å) Non-MXene system with Tc=9.18K. But Nb_2C MXene Phase has higher Tc≈12.K with relatively larger c-LP (22.7Å) with its 2D nature. Moreover, no impurity phase has been diagnosed by XRD results as well. It is interesting to note that such high Tc is observed in Mo2C MXene which suggests that such high Tc is due to the 2D nature itself not because of any impurity phase. In present case Tc is close to the predicted one for Mo_2C with generalized value of (n) for $M_{n+1}X_n$ MXenes. Such high Tc can be attributed due to strong electron-phonon coupling strengths. Large coherence length in the present case is due to strong electron-phonon coupling among the cooper pairs thus giving a constant current density over a wide range. This unique behavior in Nb_2C MXene is significant in terms of 2D superconductors as the existance of superconductivity is intrinsic to its nature. Density Functional Theory (DFT) calculations also predicts the large density of states near to the fermi level that can enhance Tc. It was further pointed out that the presence of metallic elements is the prerequisite of superconductivity in layered system. So, here all the metals are metallic in nature and it's a layered system satisfying an important condition to be a superconductive. [110, 120]

Chapter 5 Conclusions

Superconductivity in 2D materials is one of the hot topics of the research now a day. Recently discovered 2D materials known as MXenes are supposed to be superconductor especially their parent phases were reported too. CVD grown 2D structures of Such MXenes were reported to be superconductor but no practical efforts have been done before on unveiling the superconductivity in as-prepared MXene powder. This work unveils the existance of high temperature superconductivity in as-prepared MXene Powder.

The material explored in this work is two dimensional transition metal carbide known as MXene ($M_{n+1}X_n$). Two dimensional layered Nb_2C-MXene was derived from its Nb_2AlC MAX-phase with general formula $M_{n+1}AX_n$ (while, "M" is early transition metal, "A" is mainly group IIIA/IVA element i.e. group 13 or 14 and "X" is carbide/nitride or carbonitride). The etching was done simply by immersing the MAX powder into Hydrofluoric acid (40-50%) at an optimized time of 30hrs at different temperature ranging from 30°C to 50°C. etched powder washed with Deionized water and vacuum dried 80°C.

Structural analysis was carried out by XRD, SEM, EDX, Raman Spectroscopy and UV-Visible spectroscopy. The successful etching is confirmed by XRD spectrum and lamellar structure could be seen through SEM. Raman spectra indicated the removal of "Al" and bond stretching due to some terminations. Such terminations are unavoidable in chemical treatment processes which are also indicted by EDX as well. UV-Visible spectra suggest this MXene is semiconductor while DFT calculations suggest its metallic nature. The difference can be attributing to the presence of surface terminations.

For Magnetic measurements, the as-prepared powder was analyzed by SQUID (Quantum Design, MPMS) at different temperatures and Field strengths. Magnetization vs. Temperature (M-T) measurements indicates a phase transition at T_c^{onset} (K) =12.5K for normal to superconducting state. Further exploration was carried out by M-H loops at 5K, 10K and 20K. M-H loops at low temperature stipulate a typical behavior of Type-II superconductors. The flux pinning amongst the grains is stronger at low temperature and vortex state is building up more strongly at lower temperature. The superconducting diamagnetism at this temperature is more prominent by broader MH-Loops thus being consistent with M-T curves. The existance of lower and upper Critical fields is fundamental to Type-II

superconductors. Critical fields were obtained by MH-loops from zero to positive maximum fields. Ginzburg-Landau (GL) theory fitted exceptionally well with the experimentally obtained value of lower and upper critical fields thus indicating the fundamental characteristics of Type-II superconductors. Bean's Model was used to calculate the critical current density (Jc) at 5K and 10K. The enhanced critical density at low temperature results in enhanced supper current inside the material, thus inducing a strong diamagnetic behavior at that temperature, again consistent with broader MH-Loop and Separation of ZFC-FC curve at low temperature. Hence, it is concluded that

As-prepared Nb$_2$C-MXene is Type-II superconductor with Highest "Tc"

Reported till date which is close to theoretically predicted value. Such high "Tc" can be attributed to strong electron-phono coupling and high density of state (DOS) near fermi level.

Bibliography

[1] Luby Š, Lubyová M, Šiffalovič P, Jergel M, Majková E. A Brief History of Nanoscience and Foresight in Nanotechnology. In Nanomaterials and Nanoarchitectures 2015 (pp. 63-86). Springer, Dordrecht.

[2] Sengupta A, Sarkar CK, editors. Introduction to nano: basics to nanoscience and nanotechnology. Springer; 2015 Jul 1.

[3] Society, R., Nanoscience, and Nanotechnologies: Opportunities and Uncertainties: Summary and Recommendations. Royal Society: **2004**.

[4] Tolochko, N. "History of nanotechnology." Encyclopedia of Life Support Systems (EOLSS) (2009).

[5] Hulla JE, Sahu SC, Hayes AW. Nanotechnology: History and future. Human & experimental toxicology. 2015 Dec;34(12):1318-21.

[6] M.L. Minsky, Where is our microtechnology? in: The Scientist Speculates, I.J. Good, (Ed.), Heinemann, London, 1962, pp. 139.

[7] Taniguchi, Norio, Chuichi ARAKAWA, and Toshio KOBAYASHI. "On the basic concept of 'nano-technology'." Proceedings of the International Conference on Production Engineering, 1974-8. Vol. 2. 一般社団法人日本機械学会, 1974.

[8] Eric, Drexler K. "Engines of Creation. The Coming Era of Nanotechnology." Anchor Book (1986).

[9] Foresight Institute, About the Foresight Institute, http://www.foresight.org/about/index.html

[10] Katsnelson, Mikhail I. "Graphene: carbon in two dimensions." Materials today 10.1-2 (2007): 20-27

[11] Naguib, Michael, et al. "Two-dimensional nanocrystals produced by exfoliation of Ti_3AlC_2." Advanced Materials 23.37 (2011): 4248-4253.

[12] Poole Jr, Charles P., and Frank J. Owens. Introduction to nanotechnology. John Wiley & Sons, 2003.

[13] Roco, M. C., R. S. Williams, and P. Alivisatos. "Nanotechnology research directions: vision for the next decade. National Science and Technology Council, Washington, DC." (2000).

[14] Lövestam, G., et al. "Considerations on a Definition of Nanomaterial for Regulatory Purposes, JRC Reference Reports." European Commission Joint Research Centre(2010).

[15] Arivalagan, K., et al. "Nanomaterials and its potential applications." Int. J. ChemTech Res 3.2 (2011): 534-538.

[16]   Gleiter H. Nanostructured materials: basic concepts and microstructure. Acta materialia. 2000 Jan 1;48(1):1-29.

[17]   Skorokhod VV, Uvarova IV, Ragulya AV. Physico-chemical kinetics in nanostructured systems. Kyiv: Academperiodica. 2001;1:180-92.

[18]   https://www.quora.com/What-is-the-difference-between-one-two-three-and-zero-dimensional-nanomaterials

[19]   Patricia I. Dolez, Chapter 1 , Nanomaterials Definitions, Classifications, and Applications, Editor(s): Patricia I. Dolez, Nanoengineering, Elsevier, 2015, Pages 3-40, ISBN 9780444627476.

[20]   Mørup S, Frandsen C, Hansen MF. Magnetic properties of nanoparticles. InOxford Handbook of Nanoscience and Technology 2010 Dec 21.

[21]   Guimaraes AP, Oliveira IS. Magnetism and Magnetic Resonance in Solids; Wiley&Sons Inc.

[22]   Puri RK, Babbar VK. Solid state physics and electronics. S. Chand; 1998, chapter VIII, page 226.

[23]   http://www.irm.umn.edu/hg2m/hg2m_b/hg2m_b.html

[24]   http://hyperphysics.phy-astr.gsu.edu/hbase/Solids/ferro.html#c2

[25]   http://www.themagnetguide.com/magnetic-materials.html

[26]   Özgür Ü, Alivov Y, Morkoç H. Microwave ferrites, part 1: fundamental properties. Journal of materials science: Materials in electronics. 2009 Sep 1; 20(9):789-834.

[27]   https://www.nanowerk.com/spotlight/id40843_2l.jpg

[28]   Van Delft, Dirk, and Peter Kes. "The discovery of superconductivity." Physics Today 63.9 (2010): 38-43.

[29]   Bardeen J, Cooper LN, Schrieffer JR. Microscopic theory of superconductivity. Physical Review. 1957 Apr 1;106(1):162.

[30]   Gallop JC. SQUIDs, the Josephson effects and superconducting electronics. Routledge; 2017 Oct 19.

[31]   https://home.cern/science/engineering/superconductivity

[32]   http://hyperphysics.phy-astr.gsu.edu

[33]   Kamihara Y, Watanabe T, Hirano M, Hosono H. Iron-based layered superconductor La $[O_{1-x}F_x]$ FeAs (x= 0.05− 0.12) with T_c= 26 K. Journal of the American Chemical Society. 2008 Mar 19;130(11):3296-7.

[34]   https://en.wikipedia.org/wiki/Superconductivity#cite_note-1

[35]   K. S. Novoselov , D. Jiang , F. Schedin , T. J. Booth , V. V. Khotkevich , S. V. Morozov , A. K. Geim Proc. Natl. Acad. Sci. USA 2005 , 102 , 10451 .

[36]   Coleman, Jonathan N., et al. "Two-dimensional nano sheets produced by liquid exfoliation of layered materials." Science331.6017 (2011): 568-571.

[37]   Nowotny, Von Hans. "Strukturchemie einiger verbindungen der übergangsmetalle mit den elementen C, Si, Ge, Sn." Progress in Solid State Chemistry 5 (1971): 27-70.

[38]   Nowotny, Hans, Peter Rogl, and Julius C. Schuster. "Structural chemistry of complex carbides and related compounds." Journal of Solid State Chemistry 44.1 (1982): 126-133.

[39]   Barsoum, Michel W., and Tamer El-Raghy. "Synthesis and characterization of a remarkable ceramic: Ti_3SiC_2." Journal of the American Ceramic Society 79.7 (1996): 1953-1956.

[40]   Naguib, Michael, et al. "Two-dimensional nanocrystals produced by exfoliation of Ti_3AlC_2." Advanced Materials 23.37 (2011): 4248-4253.

[41]   M. Naguib , M. Kurtoglu , V. Presser , J. Lu , J. Niu , M. Heon , L. Hultman , Y. Gogotsi , M. W. Barsoum , Adv. Mater. 2011, 23, 4248.

[42]   M. Naguib , O. Mashtalir , J. Carle , V. Presser , J. Lu , L. Hultman , Y. Gogotsi , M. W. Barsoum , ACS Nano 2012 , 6 , 1322 .

[43]   Naguib, Michael, et al. "New two-dimensional niobium and vanadium carbides as promising materials for Li-ion batteries." Journal of the American Chemical Society 135.43 (2013): 15966-15969.

[44]   Barsoum, M. W., MAX Phases: Properties of Machinable Ternary Carbides and Nitrides. John Wiley & Sons: Weinheim, Germany, 2013.

[45]   Gogotsi Y. Nanomaterials handbook. CRC press; 2017 Aug 9.

[46]   Halim, J.; Lukatskaya, M. R.; Cook, K. M.; Lu, J.; Smith, C. R.; Näslund, L.-Å.; May, S. J. et al. Transparent conductive two-dimensional titanium carbide epitaxial thin films. Chem. Mater. 2014, 26 (7), 2374–2381.

[47]   Ghidiu, M.; Lukatskaya, M. R.; Zhao, M.-Q.; Gogotsi, Y.; Barsoum, M. W., Conductive two dimensional titanium carbide "clay" with high volumetric capacitance. Nature 2014, 516 (7529), 78–81.

[48]   Shahzad, Faisal, et al. "Electromagnetic interference shielding with 2D transition metal carbides (MXenes)." Science353.6304 (2016): 1137-1140.

[49]   Liu, Zhuang, et al. "2D magnetic titanium carbide MXene for cancer theranostics." Journal of Materials Chemistry B 6.21 (2018): 3541-3548.

[50]   Ghidiu, Michael, et al. "Synthesis and characterization of two-dimensional Nb_4C_3 (MXene)." Chemical communications50.67 (2014): 9517-9520.

[51]   Naguib, Michael, et al. "New two-dimensional niobium and vanadium carbides as promising materials for Li-ion batteries." Journal of the American Chemical Society 135.43 (2013): 15966-15969.

[52]   Mashtalir, Olha, et al. "Amine-assisted delamination of Nb_2C MXene for Li-ion energy storage devices." Advanced Materials 27.23 (2015): 3501-3506.

[53]   Byeon, Ayeong, et al. "Lithium-ion capacitors with 2D Nb_2CT_x (MXene)–carbon nanotube electrodes." Journal of Power Sources 326 (2016): 686-694.

[54]   Zhang, Chuanfang, et al. "Synthesis and charge storage properties of hierarchical niobium pentoxide/carbon/niobium carbide (MXene) hybrid materials." Chemistry of Materials28.11 (2016): 3937-3943.

[55]   Lin, Han, et al. "A two-dimensional biodegradable niobium carbide (MXene) for photothermal tumor eradication in NIR-I and NIR-II biowindows." Journal of the American Chemical Society 139.45 (2017): 16235-16247.

[56]   Halim, Joseph, et al. "Synthesis of two-dimensional $Nb_{1.33}C$ (MXene) with randomly distributed vacancies by etching of the quaternary solid solution $(Nb_{2/3}Sc_{1/3})_2AlC$ MAX phase." ACS Applied Nano Materials 1.6 (2018): 2455-2460.

[57]   Han, Xiaoxia, et al. "Therapeutic mesopores construction on 2D Nb_2C MXenes for targeted and enhanced chemo-photothermal cancer therapy in NIR-II biowindow." Theranostics 8.16 (2018): 4491.

[58]   Peng, Chao, et al. "A hydrothermal etching route to synthesis of 2D MXene (Ti_3C_2,Nb_2C): Enhanced exfoliation and improved adsorption performance." Ceramics International44.15 (2018): 18886-18893.

[59]   Tu, Shaobo, et al. "MXene-Derived Ferroelectric Crystals." Advanced Materials 31.14 (2019): 1806860.

[60]   Halim, Joseph, et al. "Electronic and optical characterization of 2D Ti_2C and Nb_2C (MXene) thin films." Journal of Physics: Condensed Matter 31.16 (2019): 165301.

[61]   Finkel, P., et al. "Magnetotrasport properties of the ternary carbide Ti_3SiC_2: Hall Effect, magnetoresistance, and magnetic susceptibility." Physical Review B 65.3 (2001): 035113.

[62]   Finkel, P., et al. "Low-temperature transport properties of Nano laminate Ti_3AlC_2 and Ti_4AlN_3." Physical Review B67.23 (2003): 235108.

[63]   Finkel, P., et al. "Electronic, thermal, and elastic properties of $Ti_3Si_{1-x}Ge_xC_2$ solid solutions." Physical Review B 70.8 (2004): 085104.

[64]   Hettinger, J. D., et al. "Electrical transport, thermal transport, and elastic properties of M_2AlC (M= Ti, Cr, Nb, and V)." Physical Review B 72.11 (2005): 115120.

[65]   Scabarozi, T. H., et al. "Electrical, thermal, and elastic properties of the MAX-phase Ti_2SC." Journal of Applied Physics 104.3 (2008): 033502.

[66]   Halim, Joseph, et al. "Transparent conductive two-dimensional titanium carbide epitaxial thin films." Chemistry of Materials26.7 (2014): 2374-2381.

[67]   Halim, Joseph, et al. "Synthesis and characterization of 2D molybdenum carbide (MXene)." Advanced Functional Materials 26.18 (2016): 3118-3127.

[68]   Kumar, Hemant, et al. "Tunable magnetism and transport properties in nitride MXenes." ACS nano 11.8 (2017): 7648-7655.

[69]   Hart, James L., et al. "Control of MXenes' electronic properties through termination and intercalation." Nature communications10.1 (2019): 522.

[70]   Bortolozo, A. D., et al. "Superconductivity in the Nb_2SnC compound." Solid state communications 139.2 (2006): 57-59.

[71]   Lofland, S. E., et al. "Electron-phonon coupling in $M_{n+1}AXn$-phase carbides." Physical Review B 74.17 (2006): 174501.

[72]   Bortolozo, A. D., et al. "Superconductivity in the hexagonal-layered Nanolaminates Ti_2InC compound." Solid State Communications 144.10-11 (2007): 419-421.

[73]   Bortolozo, A. D., et al. "Superconductivity in Nb_2InC." Physica C: Superconductivity 469.7-8 (2009): 256-258.

[74]   Scabarozi, T. H., et al. "Synthesis and characterization of Nb_2AlC thin films." Thin Solid Films 517.9 (2009): 2920-2923.

[75]   Bortolozo, A. D., et al. "Superconductivity at 7.3 K in Ti_2InN." Solid State Communications 150.29-30 (2010): 1364-1366.

[76]   Kuchida, S., et al. "Superconductivity in Lu_2SnC." Physica C: superconductivity 494 (2013): 77-79.

[77]   Hadi, M. A., et al. "New MAX phase superconductor Ti_2GeC: A first-principles study." Journal of Scientific Research 6.1 (2014): 11-27.

[78]   Xu, Chuan, et al. "Large-area high-quality 2D ultrathin Mo_2C superconducting crystals." Nature materials 14.11 (2015): 1135.

[79]   Wang, Libin, et al. "Magnetotransport properties in high-quality ultrathin two-dimensional superconducting Mo2C crystals." ACS nano 10.4 (2016): 4504-4510.

[80]   Zhang, Jun-Jie, and Shuai Dong. "Superconductivity of monolayer Mo_2C: The key role of functional groups." The Journal of chemical physics 146.3 (2017): 034705.

[81]   Lei, Jincheng, Alex Kutana, and Boris I. Yakobson. "Predicting stable phase monolayer Mo_2C (MXene), a superconductor with chemically-tunable critical temperature." Journal of Materials Chemistry C 5.14 (2017): 3438-3444.

[82]   Zhang, Zongyuan, et al. "Layer-Stacking, Defects, and Robust Superconductivity on the Mo-Terminated Surface of Ultrathin Mo_2C Flakes Grown by CVD." Nano letters (2019).

[83]   Arole, V. M., and S. V. Munde. "Fabrication of nanomaterials by top-down and bottom-up approaches-an overview." Journal of Materials Science 1 (2014): 89-93.

[84]   http://en.wikipedia. org/wiki/Bragg's law

[85]   Sengupta, Amretashis, and Chandan Kumar Sarkar, eds. Introduction to nano: basics to nanoscience and nanotechnology. Springer, 2015.

[86]   http://hyperphysics.phy-astr.gsu.edu/hbase/quantum/xtube.html

[87]   Inkson, B. J. "Scanning electron microscopy (SEM) and transmission electron microscopy (TEM) for materials characterization." Materials characterization using nondestructive evaluation (NDE) methods. Woodhead Publishing, 2016. 17-43.

[88]   https://blog.phenom-world.com/what-is-sem.

[89]   Ferraro, John R. Introductory raman spectroscopy. Elsevier, 2003.

[90]   Spiro, Thomas G., ed. Resonance Raman spectra of polyenes and aromatics. Vol. 2. John Wiley & Sons, 1987.

[91]   Andrews, David. Applied Laser Spectroscopy: Techniques, Instrumentation and Applications. VCH, 1992.

[92]   Chatwal, Gurdeep R., and Sham K. Anand. Instrumental Methods of Chemical Analysis:(for Hons. and Post-graduate Students of Indian and Foreign Universities). Himalaya publishing house, 1979.

[93]   Weckhuysen, Bert M. "Ultraviolet-visible spectroscopy." (2004): 255-270.

[94]   Blake Wells, David McIntyre /Ph.D. Thesis / Oregon State University/ 2015.

[95]   Clarke, John, and Alex I. Braginski. The SQUID handbook. Vol. 1. Weinheim:: Wiley-Vch, 2004.

[96]   Clarke, John, "SQUIDs", Scientific American 271, #2, August 1994, p 46.

[97]   http://hyperphysics.phy-astr.gsu.edu/hbase/Solids/Squid.html#c3

[98]   Gramm, K., L. Lundgren, and O. Beckman. "Squid magnetometer for mangetization measurements." Physica Scripta 13.2 (1976): 93.

[99]   Design, Quantum. "Magnetic Property Measurement System SQUID VSM User's Manual." (2010).

[100]   Schroder, Dieter K. Semiconductor material and device characterization, John Wiley & Sons, 2015.

[101]   Champagne, Aurélie, et al. "Electronic and vibrational properties of V_2C-based MXenes: From experiments to first-principles modeling." Physical Review B 97.11 (2018): 115439.

[102]   Hu, Tao, et al. "Vibrational properties of Ti_3C_2 and $Ti_3C_2T_2$ (T= O, F, OH) monosheets by first-principles calculations: a comparative study." Physical Chemistry Chemical Physics17.15 (2015): 9997-10003.

[103]   Rakhi, Raghavan B., et al. "Effect of postetch annealing gas composition on the structural and electrochemical properties of Ti_2CT_x MXene electrodes for supercapacitor applications." Chemistry of Materials 27.15 (2015): 5314-5323.

[104]   Yoon, Yeoheung, et al. "Low temperature solution synthesis of reduced two dimensional Ti_3C_2 MXenes with paramagnetic behaviour." Nanoscale 10.47 (2018): 22429-22438.

[105]   Su, Tongming, et al. "One-Step Synthesis of Nb_2O_5/C/Nb_2C (MXene) Composites and Their Use as Photocatalysts for Hydrogen Evolution." ChemSusChem 11.4 (2018): 688-699.

[106]   Wang, Kai. "Laser based fabrication of graphene." Advances in Graphene Science (2013): 77-95.

[107]   Yang, Jinghai, et al. "Blue-shift of UV emission in ZnO/graphene composites." Journal of Alloys and Compounds556 (2013): 1-5.

[108] Champagne, Aurélie, et al. "First-order Raman scattering of rare-earth containing i-MAX single crystals $(Mo_{2/3}RE_{1/3})_2$ AlC (RE= Nd, Gd, Dy, Ho, Er)." Physical Review Materials 3.5 (2019): 053609.

[109] Takano, Y., et al. "Superconducting properties of MgB_2 bulk materials prepared by high-pressure sintering." Applied Physics Letters 78.19 (2001): 2914-2916.

[110] Blatter, Gianni, et al. "Vortices in high-temperature superconductors." Reviews of Modern Physics 66.4 (1994): 1125.

[111] Bardeen, John, and M. J. Stephen. "Theory of the motion of vortices in superconductors." Physical Review 140.4A (1965): A1197.

[112] Joshi, Amish G., et al. "Magnetization studies on superconducting MgB_2– lower and upper critical fields and critical current density." Solid state communications 118.9 (2001): 445-448.

[113] Tiwari, Brajesh, et al. "PdTe: a 4.5K type-II BCS superconductor." Superconductor Science and Technology 28.5 (2015): 055008.

[114] http://hyperphysics.phy-astr.gsu.edu/hbase/Solids/chrlen.html#c3

[115] Kırat, G., O. Kızılaslan, and M. A. Aksan. "Effect of the Er-substitution on critical current density in glass-ceramic $Bi_2Sr_2Ca_2$ $(Cu_{3-x}Erx)O1_{0+\delta}$ superconducting system." Ceramics International 42.13 (2016): 15072-15076.

[116] Bean, Charles P. "Magnetization of high-field superconductors." Reviews of modern physics 36.1 (1964): 31.

[117] Mumtaz, M., et al. "Magneto-transport properties of Co_3O_4 nanoparticles added $(Cu_{0.5}Tl_{0.5})Ba_2Ca_2Cu_3O_{10-\delta}$ superconducting phase." Physica B: Condensed Matter 537 (2018): 283-289.

[118] Farhadi, Saeid, Kolsoum Pourzare, and Shokooh Sadeghinejad. "Simple preparation of ferromagnetic Co 3 O 4 nanoparticles by thermal dissociation of the [Co II (NH 3) 6](NO 3) 2 complex at low temperature." Journal of Nanostructure in Chemistry 3.1 (2013): 16.

[119] Hardy, George F., and John K. Hulm. "The superconductivity of some transition metal compounds." Physical Review 93.5 (1954): 1004.

[120] Lei, Jincheng, Alex Kutana, and Boris I. Yakobson. "Predicting stable phase monolayer Mo_2C (MXene), a superconductor with chemically-tunable critical temperature." Journal of Materials Chemistry C 5.14 (2017): 3438-3444.